How to Cite:
Yutsis, V.; Rapoport, Y.; Grimalsky, V.; Grytsai, A.; Ivchenko, V.; Petrishchevskii, S.; Fedorenko, A.; Krivodubskij, V. ULF Activity in the Earth Environment: Penetration of Electric Field from the Near-Ground Source to the Ionosphere under Different Configurations of the Geomagnetic Field. *Atmosphere* 2021, *12*, 801. https://doi.org/10.3390/atmos12070801

atmosphere

MDPI

Article

ULF Activity in the Earth Environment: Penetration of Electric Field from the Near-Ground Source to the Ionosphere under Different Configurations of the Geomagnetic Field

Vsevolod Yutsis [1], Yuriy Rapoport [2,3,*], Volodymyr Grimalsky [4], Asen Grytsai [2], Vasyl Ivchenko [2], Sergei Petrishchevskii [2,*], Alla Fedorenko [2,5] and Valery Krivodubskij [6]

1 División de Geociencias Aplicadas, Instituto Potosino de Investigación Científica y Tecnológica, Camino a la Presa San José #2055, San Luis Potosí 78216, S.L.P, Mexico; vsevolod.yutsis@ipicyt.edu.mx
2 Faculty of Physics, Taras Shevchenko National University of Kyiv, 03022 Kyiv, Ukraine; assen@univ.kiev.ua (A.G.); ivchenko_v@univ.kiev.ua (V.I.); fedorenkoak@gmail.com (A.F.)
3 National Center for Control and Testing of Space Facilities of the State Space Agency of Ukraine, 01010 Kyiv, Ukraine
4 Centro de Investigación en Ingeniería y Ciencias Aplicadas, Universidad Autónoma del Estado de Morelos, Cuernavaca 62209, Mor., Mexico; volodymyr.grimalsky@uaem.edu.mx
5 Space Research Institute of National Academy of Sciences of Ukraine and State Space Agency of Ukraine, 03680 Kyiv, Ukraine
6 Astronomical Observatory, Taras Shevchenko National University of Kyiv, 04053 Kyiv, Ukraine; krivod2@ukr.net
* Correspondence: yuriy.rapoport@gmail.com (Y.R.); msergiyp@gmail.com (S.P.)

check for updates

Citation: Yutsis, V.; Rapoport, Y.; Grimalsky, V.; Grytsai, A.; Ivchenko, V.; Petrishchevskii, S.; Fedorenko, A.; Krivodubskij, V. ULF Activity in the Earth Environment: Penetration of Electric Field from the Near-Ground Source to the Ionosphere under Different Configurations of the Geomagnetic Field. *Atmosphere* **2021**, *12*, 801. https://doi.org/10.3390/atmos12070801

Academic Editor: Yuichi Otsuka

Received: 2 June 2021
Accepted: 14 June 2021
Published: 22 June 2021

Abstract: The problem with the penetration of electric fields from atmospheric near-Earth electric current sources to the ionosphere is investigated both within the dynamic simulations of the Maxwell equations in the frequency domain and within the simplified quasi-electrostatic approach. Two cases of the geomagnetic field lines are considered. The first case is the penetration of the geomagnetic field lines deeply into the magnetosphere (open field lines), whereas the second one is the return of these lines into the Earth's surface (closed field lines). The proper boundary conditions are formulated. It is demonstrated that in the case of the open field lines the results of the dynamic simulations differ essentially from the quasi-electrostatic approach, which is not valid there. In the case of the closed field lines, the results of simulations are practically the same both within the dynamic approach and within the quasi-electrostatic one. From realistic values of the densities of atmospheric electric currents ~0.1 $\mu A/m^2$, the values of the electric fields within the ionosphere *F*-layer may reach about 1–10 mV/m.

Keywords: ionosphere; earthquakes; seismo-ionospheric coupling; simulation; ULF; magnetically conjugated region

1. Introduction

The problem of the lithosphere (Earth)-atmosphere-ionosphere-magnetosphere (LEAIM) coupling has been investigated for a long time [1–22] with special attention to the preparation of natural hazards and their ionospheric effects. In particular, this concerns earthquakes (EQs), tropical cyclones, and volcanic eruptions [1–3].

The hypotheses have been formulated on electrostatic [2,4,11,14,17], electrostatic-photochemistry [4,5], quasi-static [15], electromagnetic [15,16,22], acoustic-gravity [6,12,13] and other channels of seismo-ionospheric coupling, including ones of synthetic types. Examples of physical processes making a contribution to the preparation of probable precursors of the natural hazards are radon emanation and charging aerosols [1,2], formation of charge layers in the atmosphere [10], formation of a large electric field in the mesosphere [7,8], variations of very low frequency (VLF) field in the waveguide Earth-

Ionosphere [3,5,16,22], total electron content (TEC) variations in the ionosphere [20,21], etc.; these processes, in general, are of synergetic character [6,9,15,18].

For several decades, experimental results have been accumulated and recently generalized, including targeted observations over a number of years, which unambiguously indicate the presence of seismogenic disturbances in TEC, VLF, low frequency (LF) and ultra-low frequency (ULF) ranges of electromagnetic field, surface temperature, outgoing infrared (IR) radiation, chemical potential in the lower atmosphere, ionization anomalies, etc. [2,23–27]. As it was mentioned above, a set of mechanisms of coupling, in particular seismo-ionospheric one, in the LEAIM system has been proposed; in particular electrostatic [28,29], electro-photochemical [5,30], electromagnetic [15,16], mechanical (via Acoustic-Gravity Waves (AGW)) [31] and mixed mechanical-electrical [1,15,24,25,27,32,33] mechanisms have been discussed; at the same time, most likely, that in any of the above options, the observed physical phenomena are provided, accounting for the achieving by the corresponding perturbations the amplitudes, significantly exceeding the noise level, by synergetic processes in active open nonlinear LEAIM system [6,9,15,18,33,34]. Only a synergetic approach allows one to adequately, and therefore necessarily self-consistently, determine the electric field in the lower atmosphere. Moreover, for this, it is necessary to take into account a variety of physical processes, the development of instabilities and their nonlinear limitations [9] in different regions and at different heights in the LEAIM system, as well as boundary conditions, including in the lower atmosphere [15,34]. In this work, as in [15], we do not apply such a self-consistent synergetic approach and focus on the questions formulated below about comparing the dynamic and quasi-electrostatic approaches, and for situations with different configurations of the geomagnetic field. In this work, as in [15], instead of a self-consistent consideration of the motion and dynamics of charged and uncharged components of a plasma-like medium, an external current in the lower atmosphere is specified. Hereinafter, an external current is understood as a current that characterizes a given source, which is not determined by a self-consistent calculation based on the properties of the medium in which the excitations are investigated, but "assigned" and in this sense is "external" in relation to the given system, in which perturbations are sought [35]. The consequence of this is the inevitable rejection of any claims for an adequate determination of the components of the electric field in the region where the external current is specified, i.e., in the lower atmosphere. To emphasize this, in the graphs of the vertical distribution of the electric field components given in Section 3 (Figures 5, 7, and 8), an empty space is left in the region of the lower atmosphere. The external current only simulates the real current generated in the lower atmosphere by all the physical processes taking place in a self-consistent manner, but at the same time, it makes it possible to determine the field penetrating the upper ionosphere/magnetosphere.

In the present paper, we are concentrated on electromagnetic/quasi-static channel of coupling, in particular seismogenic, in the system LEAIM. We consider the electromagnetic/quasi-static perturbations in the ionosphere as a sensitive indicator of the coupling in the system mentioned above. It is interesting to note the electric fields of what orders of magnitude are observed in different regions of the atmosphere-ionosphere and at what altitudes. In the papers [29,36,37] the measurements of the vertical electric field variations with amplitudes of order (1-few) kV/m on the ground level in the region of the preparation of strong earthquakes have been reported. In [7,38] the observations of ionospheric inhomogeneities using MF-HF (Medium Frequency–High Frequency) radar have been made; the results correspond to the presence of an effective source of a mesospheric current or an electric field with amplitude (1-few V/m) [7,38,39]. It is interesting that, as it follows from the results of the numerical modeling, electric fields with amplitude of the same order (1-few V/m) in the mesosphere correspond to the presence of the (seismogenic) vertical electric field on the lithosphere-atmosphere boundary of order (1-few) kV/m [4,36,37,39]. AIP (Advanced Ionospheric Probe) on board of FORMOSAT-5 [40] provided measurements, in particular, of ion velocities. The amplitude of a seismogenic electric field in the ionosphere has been evaluated as a value of order 1 mV/m. Seismogenic plasma bubbles observed

in the ionosphere, in accordance with the modeling [6], correspond to the presence of a near-ground external electric current with density ~1 $\mu A/m^2$ and seismogenic electric field of order (few-10) mV/m in the ionosphere. The value of electric field amplitude of the same ordering [15,41] corresponds to the observed variations of order dozens of percent in total electron content (TEC) before strong earthquakes (M > 6) as well.

In our view, the coupling in the LEAIM system should be considered generally as a dynamic problem, including the set of possible instabilities [1,6–8,18,42–47] due to the dynamic nature of the processes in the lithosphere, atmosphere, ionosphere, and magnetosphere. At least, there are diurnal temporal changes. Thus, either the Maxwell equations or equivalent ones should be used to consider the coupling of near-Earth sources with the non-uniform medium possessing the highly anisotropic conductivity. The proper boundary conditions should be applied both in the lithosphere and in the upper ionosphere/magnetosphere.

This paper is devoted to the theoretical investigation of the penetration of electromagnetic fields into the ionosphere and the magnetosphere from near-Earth current sources under different configurations of the geomagnetic field lines. The first case is the penetration of the geomagnetic field lines deeply into the magnetosphere (open field lines), whereas the second one is the return of these lines into the Earth's surface (closed field lines). The simulation is dynamic that is based on the equations for the locally horizontal components of the electric field, which are equivalent to the Maxwell ones in the frequency domain. The proper boundary conditions are formulated. They are the radiation ones, i.e., the absence of the ingoing magnetohydrodynamic waves, in the magnetosphere in the case of open field lines. In the case of closed field lines, the boundary conditions should be formulated on the Earth's surface where the field lines return.

Numerical modeling realizing the algorithm used in present paper based on combined spectral-finite different method [48–50].

Also, the problem of the penetration of the electric fields is considered within the quasi-electrostatic approach. It is demonstrated that in the case of open field lines, the results of the dynamic simulations differ essentially from the quasi-electrostatic approach. Moreover, the results within the quasi-electrostatic approximation depend on the position in the magnetosphere, where the upper boundary condition is formulated. In the case of closed field lines, the results of simulations are practically the same both within the dynamic approach and within the quasi-electrostatic one.

2. Basic Equations and Parameters

The main equations used in this paper are the Maxwell equations in the frequency domain.

The model uses two coordinate frames, shown in Figure 1, and imaginary side walls, on which zero boundary conditions are formulated. The distance between the imaginary side walls is considered to be much larger than the typical horizontal scale of the "external source" of current in the lower atmosphere $\vec{j}^{ext}$ (see Figure 1 and relation (10)).

The electromagnetic field is sought in the form $E, H \sim exp(i\omega t)$, where ω is the circular frequency, which is in the ULF range $\omega \leq 1\ s^{-1}$:

$$\begin{array}{l} \vec{\nabla} \times \vec{H} = i\frac{\omega}{c}\hat{\varepsilon}(\omega, z) \cdot \vec{E} + \frac{4\pi}{c}\vec{j}^{ext}(x, y, z); \\ \vec{\nabla} \times \vec{E} = -i\frac{\omega}{c}\vec{H}. \end{array} \quad (1)$$

In Equation (1), $\vec{j}^{ext}$ is the density of the external current, $\hat{\varepsilon}(\omega, z)$ is the dielectric permittivity of the medium. The density of the external current and the field components depend on the frequency and all coordinates x, y, z. It is assumed that the properties of the ionosphere and the lower magnetosphere depend only on the vertical coordinate associated with the Earth's surface, while in the upper magnetosphere they depend on the coordinate associated with the direction of the geomagnetic field.

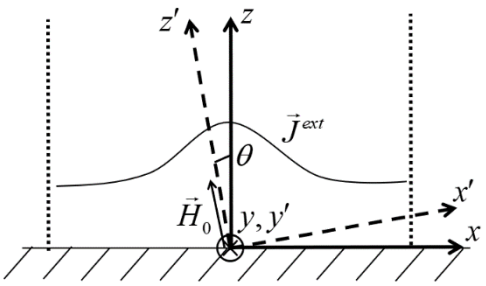

Figure 1. LEAIM system with an external current source. Imaginary side walls are shown by dashed lines. The z, z'-axes belonging to the coordinate frames shown in the figure are aligned vertically upwards and along the direction of the geomagnetic field, respectively.

In the coordinate frame $X'Y'Z'$ associated with the geomagnetic field $\vec{H}_0$ the dielectric permittivity tensor has the form [51,52]:

$$\hat{\varepsilon}'(\omega, z) = \begin{pmatrix} \varepsilon_1 & \varepsilon_h & 0 \\ -\varepsilon_h & \varepsilon_1 & 0 \\ 0 & 0 & \varepsilon_3 \end{pmatrix}, \tag{2}$$

where

$$\begin{aligned} \varepsilon_1 &= 1 - \frac{{\omega_{pi}}^2 \cdot (\omega - i\nu_i)}{((\omega - i\nu_i)^2 - {\omega_{Hi}}^2) \cdot \omega} - \frac{{\omega_{pe}}^2 \cdot (\omega - i\nu_e)}{((\omega - i\nu_e)^2 - {\omega_{He}}^2) \cdot \omega}; \\ \varepsilon_3 &= 1 - \frac{{\omega_{pi}}^2}{(\omega - i\nu_i) \cdot \omega} - \frac{{\omega_{pe}}^2}{(\omega - i\nu_e) \cdot \omega}; \; \varepsilon_h \equiv ig; \\ g &= \frac{{\omega_{pi}}^2 \cdot \omega_{Hi}}{((\omega - i\nu_i)^2 - {\omega_{Hi}}^2) \cdot \omega} - \frac{{\omega_{pe}}^2 \cdot \omega_{He}}{((\omega - i\nu_e)^2 - {\omega_{He}}^2) \cdot \omega}. \end{aligned} \tag{3}$$

The following notations are used in relations (3):

$${\omega_{pe}}^2 = \frac{4\pi e^2 n_{e0}}{m_e}, {\omega_{pi}}^2 = \frac{4\pi e^2 n_{e0}}{M_i}, \omega_{He} = \frac{eH_0}{m_e c}, \omega_{Hi} = \frac{eH_0}{M_i c}. \tag{4}$$

In (3), (4) $M_i, m_e, n_{e0}, \omega_{pe,pi}, \omega_{He,Hi}, \nu_{e,i}, H_0$ are the masses of the positive ion and electron, the concentration of electrons, the plasma frequencies of electrons and positive ions, the cyclotron frequencies of electrons and positive ions, the collision frequencies for electrons and ions, and the value of the geomagnetic field, respectively. These values depend on the height i.e., on the local vertical coordinate z. Corresponding dependencies used in modelling are shown in Section 3 (Figure 4). Hereafter, for convenience, we omit the designation of functional dependency on the height and frequency for components of dielectric permittivity tensor. The parameters of the atmosphere and the ionosphere are assumed as unchanged during the observation time. The characteristic time of essential change of the atmosphere and ionosphere parameters is of about several (3–5) hours, respectively. Frequency domain presentation is used in our paper approximately for the evaluations of the effects of electric field penetration into the ionosphere, by the order of value. We restrict ourselves by the consideration of the penetration of the electromagnetic (EM) fields from given external current sources and under given ionosphere parameters. For the other parameters, the results concerning the penetration of the electric field into the ionosphere would change, respectively.

In the coordinate frame associated with the Earth's surface, the expression for the dielectric permittivity tensor is obtained, using (2) by rotating the coordinate frame in the XOZ plane:

$$\hat{\varepsilon}(\omega, z) = \begin{pmatrix} \varepsilon_{11} & \varepsilon_{12} & \varepsilon_{13} \\ \varepsilon_{21} & \varepsilon_{22} & \varepsilon_{23} \\ \varepsilon_{31} & \varepsilon_{32} & \varepsilon_{33} \end{pmatrix}. \tag{5}$$

In relation (5), ε_{ij}; $i, j = 1, 2, 3$ are the components of the dielectric permittivity of the ionospheric plasma.

When deriving the relations for the atmosphere and the lower part of the ionosphere, the Cartesian coordinate frame is used, where the OZ axis is directed vertically upwards (Figure 1). When considering the propagation of electromagnetic fields in the upper atmosphere and magnetosphere, a set of local Cartesian coordinates associated with geomagnetic field lines within the magnetosphere is used. The approximation is that the coordinate frame is considered to be locally Cartesian, with environmental parameters that change slowly depending on the height or distance along the geomagnetic field line. The local orientation of the OZ axis is directed along the geomagnetic field line. This approximation, which is actually adiabatic, can be used due to the high anisotropy of the conductivity of the ionosphere and magnetosphere. In this case, the ULF magnetohydrodynamic (MHD) waves mainly propagate along the lines of the geomagnetic field.

Also, for wave perturbations in the ULF range, an attempt has been done to investigate the penetration of an electric field within the framework of a quasi-electrostatic approximation by means of an electric potential $\varphi \sim \exp(i\omega t)$.

$$\begin{aligned} &\vec{E} \approx -\vec{\nabla}\varphi, i\tfrac{\omega}{4\pi}\vec{\nabla}\cdot(\hat{\varepsilon}(\omega,z)\cdot\vec{\nabla}\varphi) = \vec{\nabla}\cdot\vec{j}^{ext}, \\ &\hat{\sigma}(\omega,z) \equiv i\tfrac{\omega}{4\pi}(\hat{\varepsilon}(\omega,z)-1), \\ &\vec{\nabla}\cdot(\hat{\sigma}(\omega,z)\cdot\vec{\nabla}\varphi) + i\tfrac{\omega}{4\pi}\Delta\varphi = \vec{\nabla}\cdot\vec{j}^{ext}. \end{aligned} \tag{6}$$

The fundamental difference between quasi-stationary equations (6) and the corresponding electrostatic approximation equations, which were mostly used earlier, including some of our previous works, is the presence in the last equation of system (6), of the second quasi-static, term in the left part, proportional to the frequency ω. This will allow us to investigate for the first time the possibility of the above-mentioned boundary transition between the corresponding results for electric fields using dynamic and quasi-static approximations. The following periodic zero boundary conditions for the domains along x and y are used for the numerical solution of the equations: $0 < x < L_x$, $0 < y < L_y$. Accordingly, the fast Fourier transform (FFT) is used, and the corresponding modes are represented as follows:

$$E, H, \varphi \sim \exp(-\mathrm{i}(k_x x + k_y y)). \tag{7}$$

In (7), $k_{x,y}$ are discrete wavenumbers of the corresponding Fourier modes, and for E, H, φ the amplitudes of the corresponding Fourier modes are meant, and the indices denoting the corresponding modes are omitted at the Fourier amplitudes. Then the system of two equations is obtained similarly to [15] for the column $\vec{F} \equiv (E_x, E_y)^T$. Here the superscript "$T$" means transposition, the Fourier components $E_{x,y}$ depend on the local vertical coordinate z. This system is written in the matrix form as follows:

$$\begin{aligned} &\tfrac{\partial}{\partial z}(\hat{A}_1\tfrac{\partial\vec{F}}{\partial z}) + \tfrac{\partial}{\partial z}(\hat{B}_{01}\vec{F}) + \hat{B}_{02}\tfrac{\partial}{\partial z}(\vec{F}) + \hat{B}_F\vec{F} + \\ &+\tfrac{\partial}{\partial z}(\tfrac{1}{\varepsilon_{33t}}J_z^{ext})\vec{B}_{1J_z} + \hat{B}_{2J_z}J_z^{ext}\vec{e}_F + B_{J_{tg}}\vec{J}_{tg} = 0. \end{aligned} \tag{8}$$

The matrices $\hat{A}_1, \hat{B}_{01}, \hat{B}_{02}, \hat{B}_F, \hat{B}_{2J_z}$ the vectors $\vec{B}_{1J_z}$, $\vec{e}_F$, and the values $B_{J_{tg}} = -\frac{4\pi i k_0}{c}$, ε_{33t} included in dynamic Equation (8) are presented in Appendix A (see Equations (A12)–(A17)) along with other details of the derivation of this equation. The dependencies of the matrix and vector coefficients on ω, z are omitted in Equation (8).

It is assumed in the numerical modeling that the source of external current in the lower atmosphere has only vertical component ($\vec{J}_{tg} = 0$)

$$j^{ext}(x,y,z) \equiv j_z^{ext} = j_0 \exp[-\frac{(x^2+y^2)}{{r_0}^2} - \frac{(z-z_1)^2}{{z_0}^2}]. \tag{9}$$

In relation (9), j_0, r_0, $z_{1,0}$ are the amplitude of the vertical component of the external current, the characteristic scale of the external current in the horizontal plane, the altitude position of the external current maximum, the characteristic scale of the external current in the vertical plane, respectively. Denote $L_{x,y}$ the distance between the imaginary side walls (Figure 1), which determines the periodicity of the system in the horizontal plane. Note that the boundary condition with a zero value of the tangential electric field on the imaginary sidewalls correspond to the case of a strongly localized value of the current density j_z, and the condition must be satisfied

$$r_0 << L_{x,y}. \tag{10}$$

We illustrate two physically different situations mentioned above in Figure 2. The first physical situation is with geomagnetic lines which go to the magnetosphere and do not return to the Earth (open geomagnetic field lines, Figure 2a). Boundary conditions are formulated in the magnetosphere at $z = L_z$; these are the conditions of radiation and the absence of waves propagating in the reverse direction to the ionosphere from the magnetosphere. These boundary conditions are equivalent to a system of linear relations between dE_x/dz, dE_y/dz, and E_x, E_y analogously to [15]:

$$\frac{dE_x}{dz} + m_{11}E_x + m_{12}E_y = 0; \frac{dE_y}{dz} + m_{21}E_x + m_{22}E_y = 0 \tag{11}$$

or

$$\frac{d\vec{F}}{dz} + \hat{m} \cdot \vec{F} = 0 \tag{12}$$

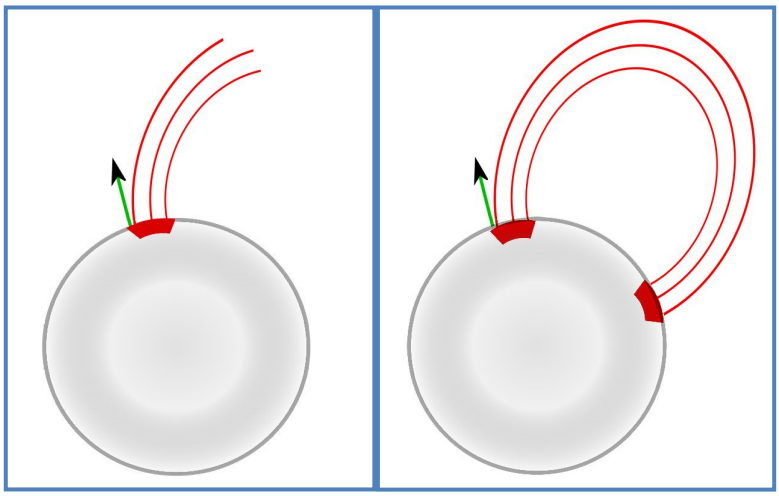

(**a**) (**b**)

Figure 2. Geometry of the problem. Part (**a**) concerns geomagnetic field lines that go to the magnetosphere and do not return to the Earth (open field lines), (**b**) the return of geomagnetic field lines to the Earth's surface (closed field lines).

Note that the matrix $\hat{m}$ included in the left side of Equation (12) consists of elements $m_{ij}; i, j = 1, 2$ that are included in the left sides of Equation (11).

The coefficients $m_{ij}, i, j = 1, 2$ included in system (11) (or, (12)) are presented in Appendix A, see relations (A38). In Appendix A, the derivation of the expressions for $m_{ij}, i, j = 1, 2$ mentioned above has been realized based on the approximation $\varepsilon_3 \to \infty$ (see relation (A18)). Nevertheless, we are interested in the comparison between the results based on the dynamic and quasi-static approaches for the determination of the electric field penetration through the system LEAIM. So, it would be quite reasonable to consider the boundary conditions (11), (12) using the more exact approach and accounting for the

existence of effectively at least *two* small parameters in the theory describing ULF waves in the upper ionosphere and magnetosphere. One of these parameters describes anisotropy and is small in the F region of ionosphere and magnetosphere and is equal to

$$|\varepsilon_1|/|\varepsilon_3|(\frac{1}{\cos^2\theta}\frac{k_x^2}{k_t^2}+\frac{k_y^2}{k_t^2}) << 1 \tag{13}$$

where

$$k_t=\sqrt{k_x^2+k_y^2}\sim L_\perp^{-1}. \tag{14}$$

In (14), $L_\perp$ is the characteristic size of the transverse distribution of the (horizontal) electric field components; the determination of k_t corresponds also to one presented after Equation (A10) in Appendix A. The other parameter is $|\varepsilon_1|(k_0^2/k_t^2)$, where $k_0=\omega/c$, and is proportional to ω, when ω is relatively small (see relation (3)).

As it follows from the accurate analysis of the Equations (A25)–(A27), the dispersion relation for Alfven waves (AWs) takes the form:

$$A_0k_z^2+2B_0k_z+C_0=0; k_{z1,2}=A_0^{-1}[-B_0\pm\sqrt{B_0^2-A_0C_0}]. \tag{15}$$

In Equation (15),

$$\begin{array}{l} A_0=\cos^2\theta+\frac{\varepsilon_1}{\varepsilon_3}\sin^2\theta;\ B_0=-k_x\cos\theta\sin\theta(1-\frac{\varepsilon_1}{\varepsilon_3});\\ C_0=k_x^2(\sin^2\theta+\frac{\varepsilon_1}{\varepsilon_3}\cos^2\theta)+\frac{\varepsilon_1}{\varepsilon_3}k_y^2-k_0^2\varepsilon_1. \end{array} \tag{16}$$

Accounting for (13), one can get, using (15), (16), more accurate expression than (A29) for AW mode:

$$\begin{array}{l} k_{za}\approx k_x\tan\theta(1-\frac{\varepsilon_1}{\varepsilon_3}\frac{1}{\cos^2\theta})\\ \pm\frac{1}{\cos\theta}(1-\frac{\varepsilon_1}{\varepsilon_3}\tan^2\theta)\sqrt{k_0^2\varepsilon_1-\frac{\varepsilon_1}{\varepsilon_3}(\frac{k_x^2}{\cos^2\theta}+k_y^2)}. \end{array} \tag{17}$$

The dispersion relation for fast magnetosonic waves (FMSW) mode has nevertheless the same form as the one presented in Equation (A30):

$$k_{zs}=\pm\sqrt{\varepsilon_1k_0^2-k_t^2}. \tag{18}$$

Consider two cases, corresponding to the different ratios between the two parameters mentioned above. Namely, the first of them describes the anisotropy (see relation (13)). The second one is $|\varepsilon_1|(k_0^2/k_t^2)$ and is small and proportional to ω for relatively small frequency, as mentioned above.

(1) In the first case, suppose that both parameters are small, and the condition

$$|\varepsilon_1|\frac{k_0^2}{k_t^2}<\frac{|\varepsilon_1|}{|\varepsilon_3|}(\frac{1}{\cos^2\theta}\frac{k_x^2}{k_t^2}+\frac{k_y^2}{k_t^2}) << 1 \tag{19}$$

is satisfied. Under the condition (19), Equations (17) and (18) reduce to

$$k_{za}\approx k_x\tan\theta\pm\frac{1}{\cos\theta}\sqrt{k_0^2\varepsilon_1-\frac{\varepsilon_1}{\varepsilon_3}(\frac{k_x^2}{\cos^2\theta}+k_y^2)}; k_{zs}=\pm ik_t. \tag{20}$$

Accounting for (20) and applying the approach similar to the one used in Appendix A for the derivation of the relations (A38), one can get, by the order of value, the estimation

$$\Delta z_{eff}\sim k_t^{-1}\sim L_t. \tag{21}$$

In relation (21), Δz_{eff} is the penetration depth of the MHD waves penetrating into the higher ionosphere/magnetosphere from some altitude z where the (horizontal) electric field distribution has the typical transverse size of order L_t.

(2) In the second case, suppose that, instead of (19), the second parameter $|\varepsilon_1|(k_0^2/k_t^2)$ is of order 1, the following condition is satisfied:

$$\frac{|\varepsilon_1|}{|\varepsilon_3|}\left(\frac{1}{\cos^2\theta}\frac{k_x^2}{k_t^2}+\frac{k_y^2}{k_t^2}\right) << |\varepsilon_1|\frac{k_0^2}{k_t^2} \sim 1. \tag{22}$$

In this case, the relations (17), (18) reduce in accordance with the relations (A29), (A30), to the form

$$k_{za} \approx k_x \tan\theta \pm \frac{k_0\sqrt{\varepsilon_1}}{\cos\theta};\ k_{zs} = \pm\sqrt{\varepsilon_1 k_0^2 - k_x^2}. \tag{23}$$

Let us make the estimation for $z = 200$ km, $\omega \sim 2.5 \cdot 10^{-2}\mathrm{s}^{-1}$, $|\varepsilon_1| \sim 10^7$, $L_t \sim 4000$ km (see Figures 4e and 5a,b, respectively, shown below in the Section 3). Using the relations (23), (A38), one can get

$$\Delta z_{eff} \sim \sqrt{|\varepsilon_1|}k_0 \sim 3000 \text{ km}. \tag{24}$$

The second physical situation is when geomagnetic lines return to the Earth's surface (closed geomagnetic field lines, Figure 2b). In this situation, the boundary conditions are $E_x = E_y = 0$ on the Earth's surface (or $\varphi = 0$, for a quasi-electrostatic approximation; in the case of open geomagnetic field lines in this approximation, the same boundary condition applies to the magnetosphere). Such boundary conditions on the Earth's surface correspond to the infinite conductivity of the Earth. The consideration of the finite conductivity of the solid Earth weakly changes the corresponding results, as our simulations have demonstrated.

For the solution of set of Equations (8) the matrix run method, or matrix factorization method [48–50], is used. The corresponding boundary condition (11) (or (12)), as well as zero conditions for x- and y-components of the electric field on the side walls (see Figure 1) and the lower boundary $z = 0$ are taken into account. This method is described in Appendix B. When the transverse sizes of the simulation region are quite large, the results of simulations are the same both for the zero boundary conditions at the sidewalls and for the periodic boundary conditions.

Because in the upper ionosphere and the magnetosphere the electromagnetic field propagates along the geomagnetic field lines, which are curved, the adiabatic rotation of the locally rectangular coordinate frames (c.f.) has been applied, Figure 3. Namely, near the Earth's surface OZ axis of c.f. is aligned vertically, whereas OX, OY ones are tangential to the Earth's surface. Starting from the altitude $z = z_2 \approx 300$ km, the adiabatic rotation of OZ, OX axes takes place, and at the altitude $z = z_3 \approx 600$ km OZ axis becomes aligned along the geomagnetic field line. The adiabaticity is due to the small rotation angle at each simulation step along OZ axis $h_z < 1$ km. In the case of open geomagnetic field lines, the OZ axis of the local c.f. preserves this orientation within the magnetosphere. In the case of the closed geomagnetic field lines, the inverse procedure has been realized near the return point, so in the return point at the Earth's surface, OZ axis is aligned vertically. It has been checked that the simulation results depend weakly on the positions of the points z_2, z_3, z_4, z_5.

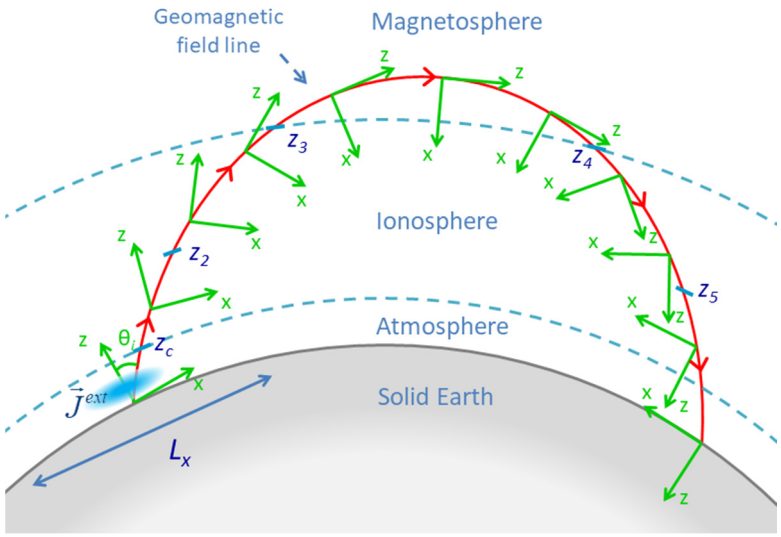

Figure 3. Adiabatically rotated coordinate frames (c.f.) in the case of closed geomagnetic field lines. The points are as follows: $z_c \approx 70$ km is the boundary between the upper atmosphere and the ionosphere, $z_2 \approx 300$ km is the point in the upper ionosphere where the adiabatic rotation of the locally rectangular coordinate frames occurs, $z_3 \approx 600$ km is the point in the lower magnetosphere where the local c.f. is aligned along the geomagnetic field line, z_4 is the point in the lower magnetosphere where the inverse rotation of c.f. starts, z_5 is the point in the upper ionosphere where OZ axis of the local c.f. is directed perpendicularly downwards to the Earth's surface near the return region. L_x is the horizontal region of simulations, j^{ext} is the density of external current.

The necessity of the application of the dynamic simulations for the problem of the penetration of the electric fields into the ionosphere is due to the following factors.

1. The atmosphere, ionosphere, and magnetosphere jointly with the current sources are principally dynamic. Especially, the increase of the electric fields in the atmosphere lasts for several minutes. The properties of the ionosphere change for several hours. The conductivity of the air near the Earth's surface is low: $\sigma < 10^{-3}$ s^{-1}, so it is necessary to take into account the influence of the nonzero frequency there, if $\omega > \omega_{00}$; $\omega_{00} \sim 3 \cdot 10^{-3}$s^{-1}.

2. When the boundary condition for the electric potential is in the deep magnetosphere L_z = 25,000 km, the deep magnetosphere itself is a dynamical system due to the Earth's rotation around the Sun. During 1 hour of rotation, the Earth moves >100,000 km in space, so the configuration of the geomagnetic field changes.

3. In the set of papers, in particular in [45], it was shown that there are definite restrictions for the applicability of the electrostatic approximation. Further transition to the quasi-static model [46] confirms the importance of accounting for the non-stationary character of the processes in the near-Earth space. In [46], it was stated that the cases of open and close (see Figure 2 in that paper) geomagnetic field lines should be treated differently. As it is shown in Appendix C for the open geomagnetic field lines, the upper boundary conditions (relations (A53)) have the structure similar to those of the upper boundary conditions [47].

In papers [17,45,47] there were estimations of limited validity of the electrostatic approximation. Then a lot of authors used a more correct term 'the quasi-statics' instead of 'the electrostatics', for instance [46] and references there.

In the paper [46], there is a clear understanding that under different configurations of the geomagnetic field lines the approaches to simulations on the penetration of the electric field with the quasi-statics should be different, especially with respect to the boundary condition from above, see for instance Figure 2 in [46].

3. The Results of Simulations

The main goal is to estimate the penetration of the electric field components to the *E*- and *F*-layers of the ionosphere under different geometries of the geomagnetic field lines.

The values of the parameters for simulations have been selected due to the considered problem as follows. As for the height $z = z_1$, at which the maximum of the external current is placed, we consider two examples. In the first of them, the current maximum is somewhat raised directly above the surface region. This study is of interest from several points of view. First, the external current in the model adopted in this work qualitatively corresponds to the effective sources associated with synergetic processes. From the point of view of the prospects of the above-mentioned synergetic approach, one should take into account the presence of a number of different instabilities at different heights in the "lithosphere-ionosphere" system, including the lower atmosphere, as well as its surface layer [42,43], the mesosphere [39], *E* [53] and *F* [1,15,33] regions of the ionosphere. Therefore, it is of interest to consider the case when the external current is raised directly above the surface layer. It should be mentioned that powerful surface sources causing a noticeable response in the ionosphere include also tropical cyclones and typhoons [1,15,33,53–57]. The kinetic energy carried by tropical cyclones is comparable to the energy of powerful earthquakes, so the tropical cyclones are among the most destructive large-scale atmospheric formations on our planet [54,56,57]. The impact of a tropical cyclone on the ionosphere is carried out by means of a mixed mechanism, including enhanced ionization, electrophysical, hydrodynamic, meteorological, and other processes. As a result of these processes, the self-organized powerful atmospheric formation is formed, namely, an atmospheric vortex. Such a vortex is a known characteristic feature of tropical cyclone. This formation has a horizontal scale of the order of hundreds to thousands of kilometers [54]. Such a formation includes structures with strong convection and clouds, so-called convective towers [58], where both forming AGWs and intense currents and fields arising due to charge separation are clearly manifested, in particular, in lightning discharges. Moreover, such electrically saturated convective structures reach heights of 16 km [59,60]. The resulting electric fields, together with AGW, affect the ionosphere, causing noticeable disturbances of the total electron content (TEC) [58], variations in the penetration frequency foF2 [61], variations in the characteristics of VLF waves propagating in the waveguide Earth-Ionosphere and other phenomena, some of which are considered now, in the processes of tropical cyclone/hurricane formation, as the corresponding precursors [62].

In accordance with the pointed above features, for the first part of simulations, it has been adopted that the electric current source is localized in the lower atmosphere, $z_1 = 14$ km, above the Earth's surface. The maximum value of the density of electric current $j_0 = 0.1$ μA/m^2, [54,56], the transverse and vertical scales $r_0 = 500$ km [54,56], and $z_0 = 7$ km [59,60] are adequate parameters, characterizing the external current source for the evaluations by the order of value.

After the calculation for a source in the lower atmosphere with an elevated maximum ($z_1 = 14$ km), a number of calculations will also be performed for different positions of the maximum of the external current source along with the height in the region $0 \leq z_1 \leq z_{01}$, $z_{01} = 14$ km. Among these calculations, some will be done for the vertical coordinate of the current source maximum, which, altogether with other parameters, would qualitatively correspond to the seismogenic source. Also, calculations based on the dynamic and quasi-electrostatic approaches will be performed for some frequencies in the ULF range, with the justification for the choice of these values.

The parameters of the atmosphere, ionosphere, and magnetosphere used in the simulations for different values of height are presented in Figure 4. The parameters of the ionosphere used for modeling are taken from [18,51,52,63–65]. The simulations are tolerant to changes in the parameters and mainly yield qualitative results.

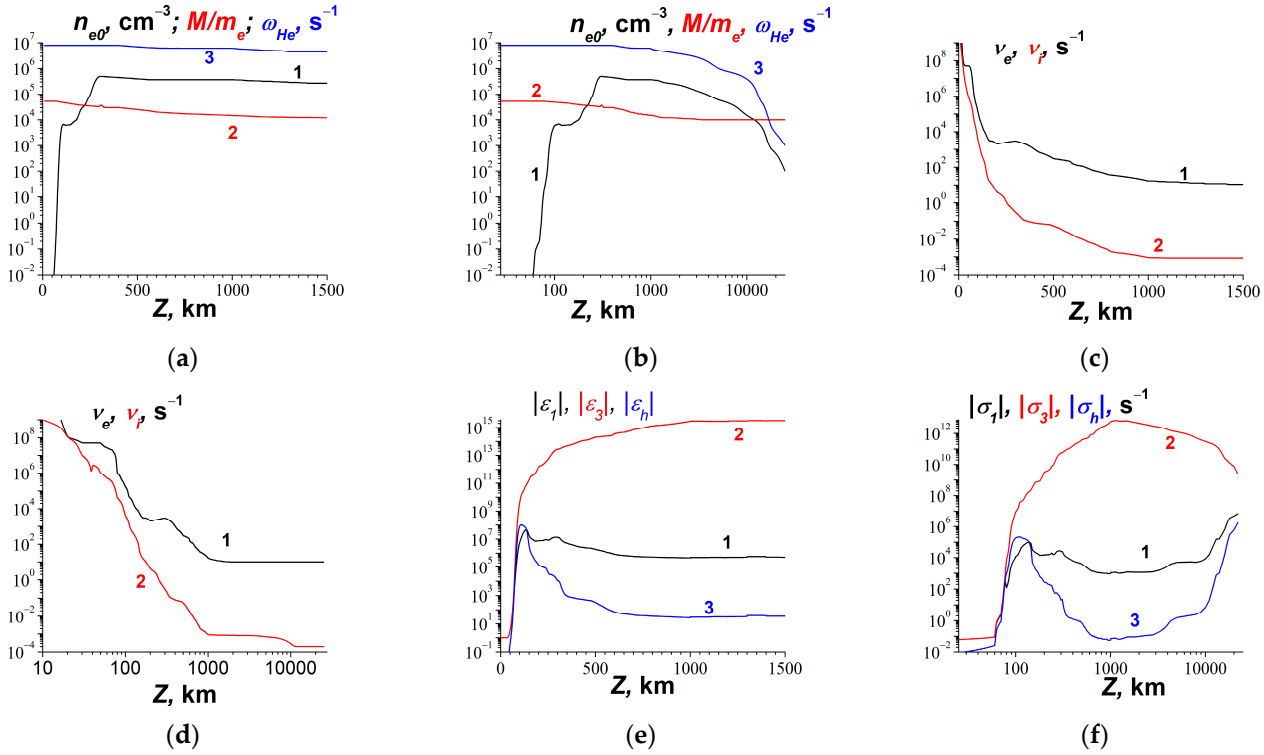

Figure 4. The dependences of the ionosphere and the magnetosphere parameters on height used in simulations. Parts (**a**,**b**) are dependencies of the electron concentration n_{e0}, the ratio of the ion mass to electron one, and the electron cyclotron frequency, curves 1, 2, 3. Parts (**c**,**d**) are dependencies of the electron and ion collision frequencies, curves 1, 2. Parts (**e**,**f**) are the absolute values of the components of the permittivity and the absolute values of the components of the complex conductivity at the frequency $\omega = 0.025$ s^{-1}. Data ate taken from the books [18,51,52,63–65].

The choice of the frequencies of the external current source located in the lower atmosphere is due to the following considerations.

(1) We compare calculations based on dynamic and quasi-electrostatic models of electric field penetration into the ionosphere and magnetosphere. In particular, we are interested in the lower frequency limit. The frequency $\omega = 2.5 \cdot 10^{-2}\text{s}^{-1}$ chosen for the calculations determines the lower frequency limit that we can practically reach at the moment in the calculations on the basis of the dynamic model. This limit is determined by the fact that decreasing model frequency two times requires a fourfold increase in Random Access Memory (RAM), during the calculations based on the dynamic approach. Despite this, we qualitatively investigate the penetration of the field into the ionosphere and magnetosphere also at frequencies $\omega < 2.5 \cdot 10^{-2}\text{s}^{-1}$ for the quasi-electrostatic approach.

As shown below, the application of the quasi-electrostatic approach is adequate for the case of closed geomagnetic field lines. Moreover, the goals of this work include clarifying the qualitative nature of the dependences of the field penetration on some parameters of the source, including its frequency. The calculation results in the dynamic and quasi-electrostatic approximations are compared in the region of minimum frequencies $\omega \sim 2.5 \cdot 10^{-2}\text{s}^{-1}$ (namely, for $\omega = 2.5 \cdot 10^{-2}\text{s}^{-1}$ and $\omega = 5 \cdot 10^{-2}\text{s}^{-1}$), in which our computational capabilities still allow us to apply not only the quasi-electrostatic approximation, which does not have, with the mathematical point of view, frequency restrictions "from below", but also a dynamic approach.

As we will demonstrate in this section, in the aforementioned boundary frequency range, where both dynamic and quasi-static approaches are applicable, they, as expected, with appropriate calculations, give for the maxima of the field components the values of the same order of magnitude. In our qualitative studies of the electric field penetration from

the lower atmosphere into the ionosphere and magnetosphere, the accuracy of determining the field components in order of magnitude is quite satisfactory.

(2) Let us take into account the existence of a correspondence, as will be shown below, in order of magnitude and in qualitative behavior depending on the height, between the results obtained in the case of closed geomagnetic field lines for the maximum field value using dynamic and quasi-electrostatic approaches. This allows, by matching the results for these two approaches in the above-designated frequency range, where they are both applicable, to "go down" in frequency on the basis of a quasi-electrostatic approach. Thus, it is possible to study the field penetration from a given (external) current source, with an accuracy of an order of magnitude, in the lower part of the ULF range.

The typical results of simulations are presented in Figures 5–10. The frequency interval is ω = 0.025–0.05 s^{-1}, where there is a possibility to apply the quasi-electrostatic approximation. The values of the electric field components are in mV/m units. The results of the simulations are of qualitative character and are tolerant to changes in the parameters of the ionosphere. The region of simulations in the locally horizontal plane *XOY* has been chosen quite large to avoid an influence of boundaries on the electric field distributions, so it should be $L_{x,y} \geq$ 10,000 km. The initial inclination of the geomagnetic field from the normal to the Earth's surface is $\theta_i = 10^\circ$. The results depend weakly on this parameter when $\theta_i < 30^\circ$.

In the case of open field lines, the results of simulations are presented in Figures 5–7 and 13. Within the dynamic simulations there exists the penetration of the horizontal electric field components to the heights $z >$ 150 km. These dependencies are presented at the heights $z \geq$ 50 km only because at lower heights the values of the electric field, especially the vertical component E_z, cannot be computed correctly in the regions where the external current source j^{ext} is not zero [15]. The used approximation of the given external current sources is too rough there [15]. Within the dynamic approach, the simulated penetration does not depend on the position of the upper boundary condition L_z, when $L_z \geq$ 1000 km, see Figure 5. Specifically, the dependencies for the upper boundary condition at L_z = 25,000 km coincide with ones for L_z = 1500 km, curves 3 in Figure 5. Also, the values of the electric field components depend slightly on the frequencies at $\omega \leq 0.1$ s^{-1}. This can be seen from Figure 6 where the spatial distributions of the electric field components are presented at z = 200 km in *F*-layer; compare Figure 6a,d (for E_x component), Figure 6b,f (for E_y component), and Figure 6c,g (for E_z component). Moreover, in the dynamic simulations for the open geomagnetic lines, the results of simulations with the adiabatic rotation of the coordinate frame (c.f.) coincide with ones without such a rotation, where the orientation of c.f. has been unchanged.

Note that under the parameters used for the modeling presented in Figures 5 and 6, the evaluation (24) is suitable and corresponds qualitatively to the results presented in the Figures mentioned above. The difference of frequency in two times leads to a difference in maxima of amplitudes of electric field components which does not exceed a value of order (compare Figure 6a–c with Figure 6d–f, respectively). In the accordance with (24), in the magnetosphere at the vertical distances $z >$ 1000 km, the maxima slowly decrease with the growth of z, as our simulations have demonstrated, but the detailed investigation of the penetration of the electromagnetic fields into the magnetosphere is out of scope of this paper.

Contrary to this, within the quasi-electrostatic approximation the simulated penetration is very poor in the ionosphere *F*-layer, 3 orders smaller than one within the dynamic simulations. The results of the quasi-electrostatic simulations are given in Figure 7. Two types of boundary conditions within the magnetosphere have been applied, namely either $\varphi = 0$ or $E_z = 0$. The results of the simulations do not depend on the types of the boundary conditions. Note that the upper condition $E_z = 0$ corresponds to the absence of the electric current along the geomagnetic field line [46]. The simulated values of the electric field depend on the position of the upper boundary condition. For the curve 1 the value of L_z is L_z = 1000 km, for curves 2, 3 they are 1500 km and 25,000 km (Figure 7). At the

distance L_z = 25,000 km along the geomagnetic field line, i.e., in the deep magnetosphere, the parameters of the magnetosphere are assumed as $n_{e0} = 10^2$ cm^{-3}, $M/m_e = 10^4$, $\omega_{He} = 10^3$ s^{-1}, $\nu_e = 10$ s^{-1}, $\nu_i = 10^{-4}$ s^{-1}, that yields the components of the conductivity $\sigma_1 \approx 3.1 \cdot 10^5 + i6.8 \cdot 10^6$, $\sigma_3 \approx 2.6 \cdot 10^9 - i1.1 \cdot 10^8$, $\sigma_h \approx -1.7 \cdot 10^6 + i2.9 \cdot 10^4$. The results of the quasi-electrostatic simulations depend weakly on changing the parameters in the deep magnetosphere.

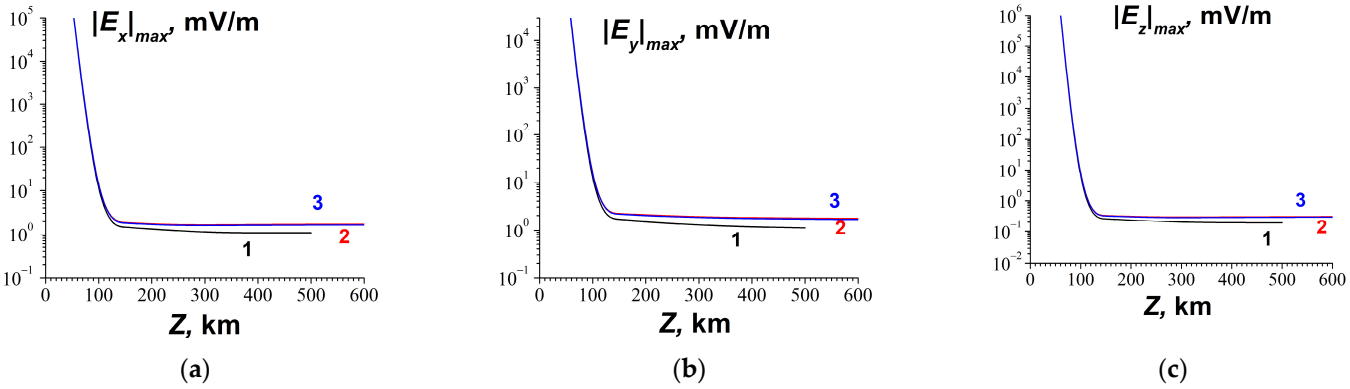

Figure 5. The dependencies of the maximum values of the electric field components E_x (**a**), E_y (**b**) and E_z (**c**) on the vertical coordinate obtained in the dynamic simulations, the frequency is $\omega = 0.025$ s^{-1}, Curve 1 is for L_z = 500 km, 2 is for L_z = 1000 km, 3 is for L_z = 1500 km. The geomagnetic field inclination is $\theta_i = 10°$. The case of open geomagnetic field lines is considered. Leaving empty space in the lower atmosphere area in Figure 5a–c and below in Figures 7, 8 and 13, corresponds to the rejection of claims for an adequate definition of the electric field in the external current region, introduced instead of an synergetic self-consistent definition of current and field, as explained in detail in the introduction to this work, as well as in [15].

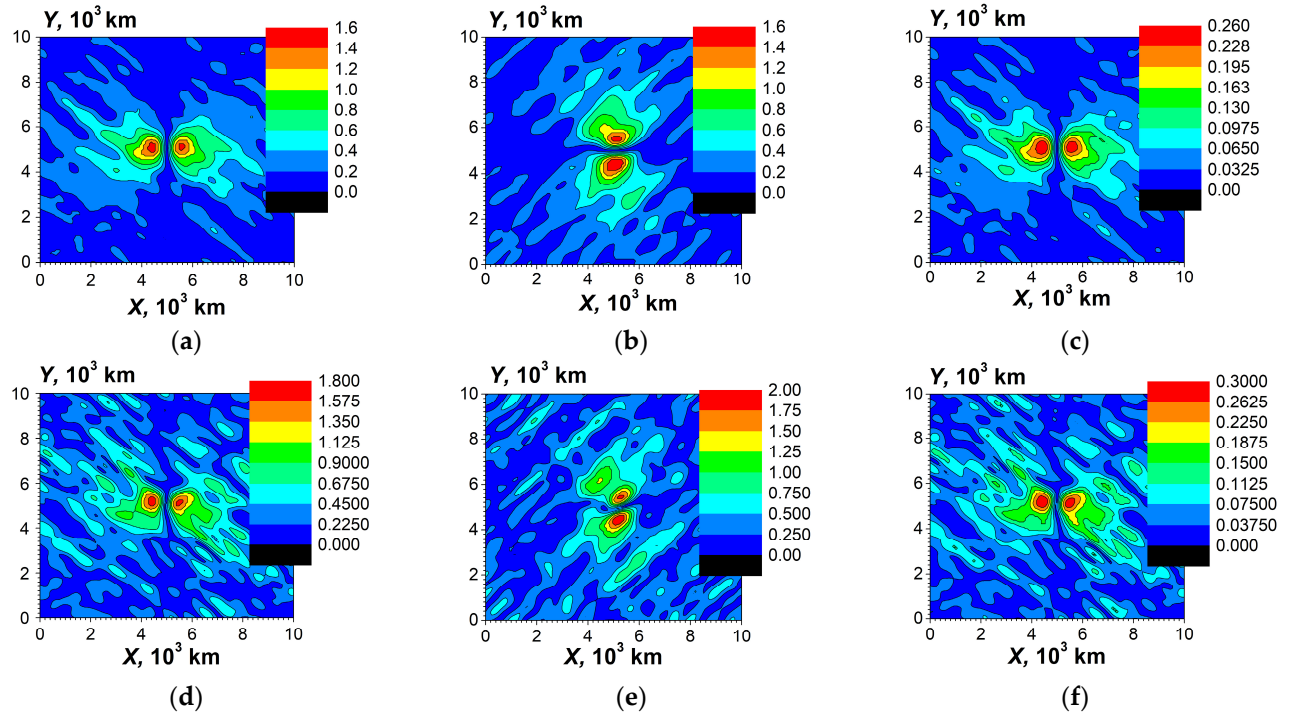

Figure 6. Distributions of the electric field components (in mV/m) in the ionosphere *F*-layer at the height z = 200 km, the dynamic simulations. The case of open geomagnetic field lines is considered here. The frequencies are $\omega = 0.05$ s^{-1}, parts (**a**–**c**), and $\omega = 0.025$ s^{-1}, parts (**d**–**f**). Parts (**a**,**d**) are $|E_x(x,y)|$, (**b**,**e**) are $|E_y(x,y)|$, (**c**,**f**) are $|E_z(x,y)|$. The total vertical distance of the simulation is L_z = 1500 km. The geomagnetic field inclination is $\theta_i = 10°$.

The explanation of the great difference between the results of the dynamic and the quasi-static approximations (compare Figures 5a–c and 7a–c, respectively) is as follows. The quasi-electrostatic approximation can be applied when the following condition of the small retardation is valid: $L_z << v_A/\omega$ [66], where $v_A = c/\varepsilon_1{}^{1/2} \approx H_0/(4\pi n_{e0}M)^{1/2}$ is the Alfven velocity [51,52]. For the rough estimations we accept the condition of the validity of quasi-electrostatic approximation in the form:

$$L_z < \frac{v_A}{2\omega}. \tag{25}$$

It is of about $v_A \approx 400$ km/s within the upper ionosphere and $v_A \approx 100$ km/s in the magnetosphere [51,52]. Thus, it should be $L_z < 2000$ km. Such a condition could not be satisfied for $L_z = 25{,}000$ km, see curves 3 in Figure 7a–c, built for the open field line and quasi-electrostatic. In the case of open geomagnetic field lines, it is seen from Figure 7 that the behavior of the electric field depends essentially on the position point L_z of the upper boundary condition, compare curves 1, 2, and 3 in Figure 7. Within the quasi-electrostatic approximation at all values of L_z the electric field in the ionosphere, *F*-layer is several orders smaller compared with the dynamic simulations, Figure 5.

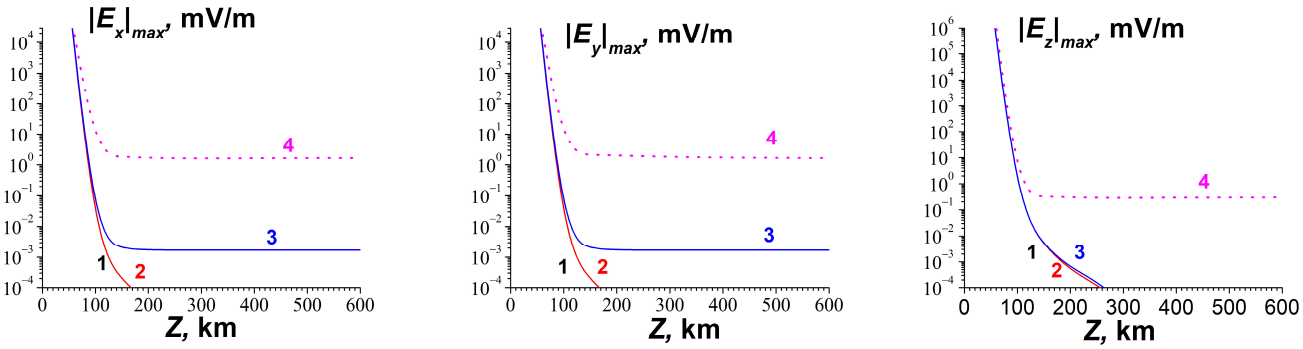

Figure 7. The dependencies of the maximum values of the electric field components on the vertical coordinate obtained in the quasi-electrostatic simulations, the same frequency $\omega = 0.025$ s^{-1}. The geomagnetic field inclination is $\theta_i = 10°$. The case of open geomagnetic field lines is considered. Curves 1 are for $L_z = 1000$ km, 2 are for $L_z = 1500$ km, 3 are for $L_z = 25{,}000$ km. For a comparison, the results of the dynamic simulations are given in curves 4 taken from Figure 5, for $L_z = 1500$ km. Leaving empty space in the lower atmosphere area as in Figure 5a–c and in Figures 7, 8 and 13, corresponds to the rejection of claims for an adequate definition of the electric field in the external current region, introduced instead of an synergetic self-consistent definition of current and field, as explained in detail in the introduction to this work, as well as in [15].

In the case of closed geomagnetic field lines, the horizontal components of the electric field penetrate into the ionosphere both within the dynamic simulations and in the quasi-electrostatic approximation. The results of simulations are given in Figures 8–12. The distance along the geomagnetic field line is $L_z = 2000$ km, i.e., it includes two parts, from the Earth's surface to the magnetosphere and back from the upper point in the magnetosphere to the Earth's surface. The values of the electric field have a correspondence in these simulations. The quasi-static approximation is approximately valid, when the total distance along the geomagnetic field line is of about 2000 km between the Earth's surfaces. The quantitative difference is due to both some non-quasi-stationarity and the roughness of the model. In this case, to get more exact results it is necessary to take into account in detail the curvature of the geomagnetic field lines under the quasi-static approximation. Under dynamic simulations, the influence of this curvature is not so essential, as our simulations have been demonstrated.

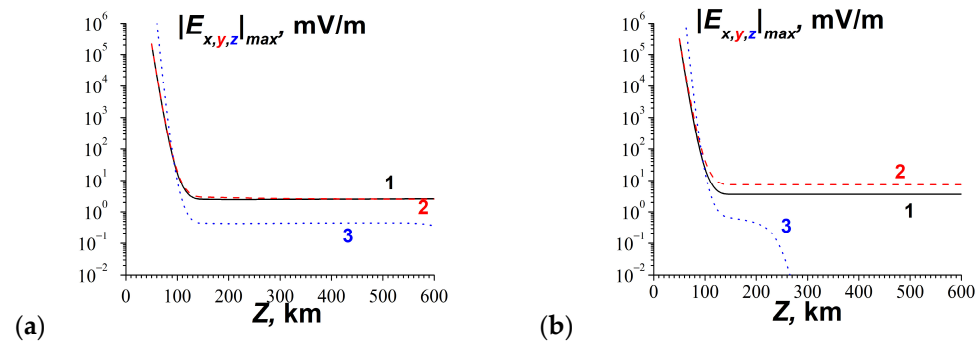

Figure 8. The dependencies of the maximum values of the electric field components on the vertical coordinate obtained in the dynamic simulations, part (**a**), and in the quasi-electrostatic ones, part (**b**). The frequency is $\omega = 0.025$ s^{-1}. The geomagnetic field inclination is $\theta_i = 10°$. The case of closed geomagnetic field lines is considered. The total vertical distance of the simulation is $L_z = 2000$ km. The curves 1, 2, 3 are the maximum values of $|E_x|$, $|E_y|$, $|E_z|$ components correspondingly. Leaving empty space in the lower atmosphere area as in Figure 5a–c and in Figures 7, 8 and 13, corresponds to the rejection of claims for an adequate definition of the electric field in the external current region, introduced instead of an synergetic self-consistent definition of current and field, as explained in detail in the introduction to this work, as well as in [15].

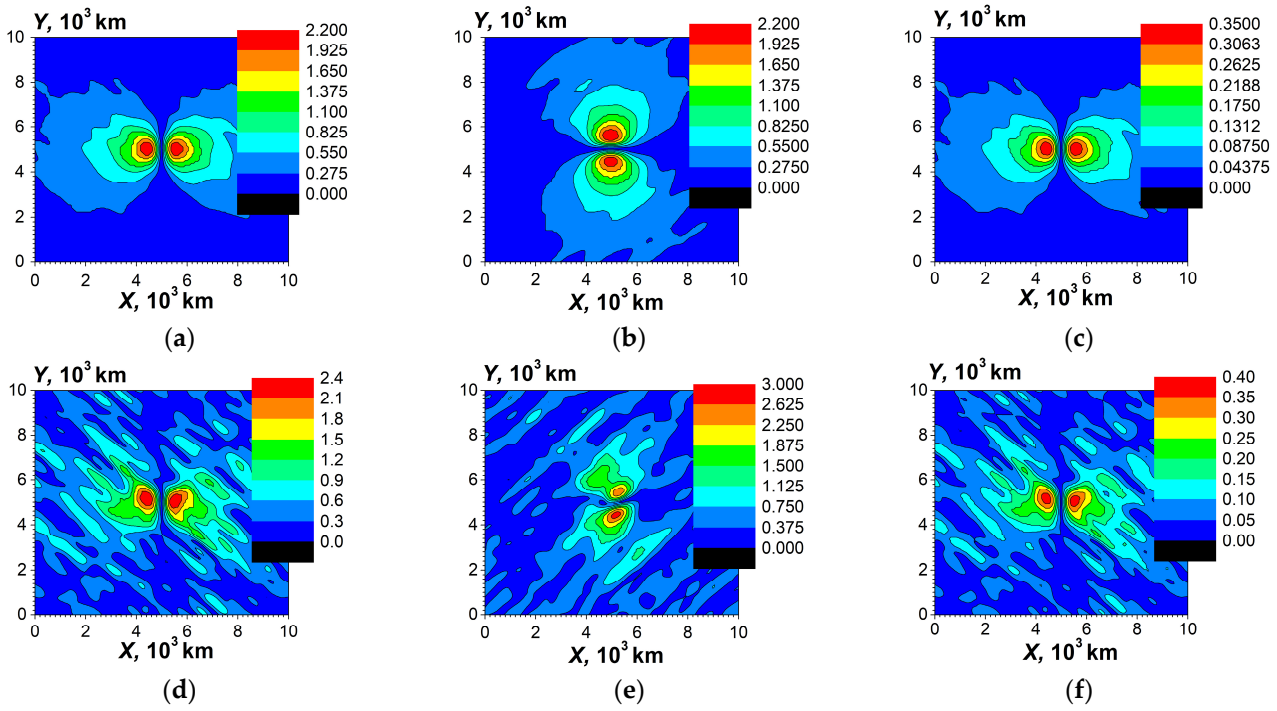

Figure 9. Distributions of the electric field components (in mV/m) in the ionosphere *F*-layer at the height $z = 200$ km. The dynamic simulations, the case of closed geomagnetic field lines. The total vertical distance of the simulation is $L_z = 2000$ km. The geomagnetic field inclination is $\theta_i = 10°$. Parts (**a**–**c**) are for $\omega = 0.05$ s^{-1}, (**d**–**f**) are for $\omega = 0.025$ s^{-1}. Parts (**a**,**d**) are $|E_x(x,y)|$,(**b**,**e**) are $|E_y(x,y)|$, (**c**,**f**) are $|E_z(x,y)|$.

As it is seen from Figure 9, parts a and d, b and e, c and f, in the case of closed geomagnetic field lines, the differences in corresponding maximum values of electric field components for the frequencies 0.05 s^{-1} and 0.025 s^{-1} does not exceed a value of order 25%.

From Figures 5 and 8 it is seen that the dynamically computed values of the electric field in the ionosphere *F*-layer are a bit higher in the case of closed geomagnetic field lines. This can be explained by a partial reflection of the magnetohydrodynamic waves from the Earth's surface in the place of returning the geomagnetic field lines.

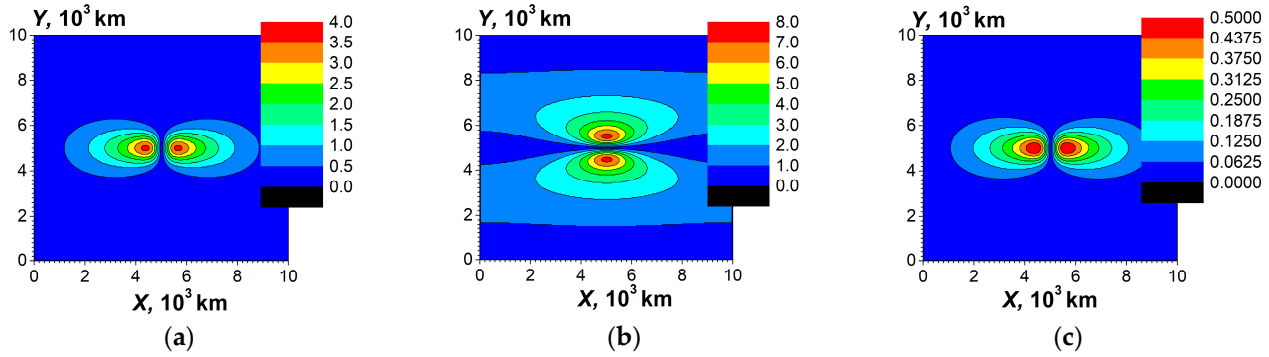

Figure 10. Distributions of the electric field components (in mV/m) in the ionosphere *F*-layer at the height z = 200 km. The quasi-electrostatic simulations, the case of closed geomagnetic field lines. The frequency is $\omega = 0.025\ s^{-1}$. Part (**a**) is $|E_x(x,y)|$, (**b**) is $|E_y(x,y)|$, (**c**) is $|E_z(x,y)|$. The inclination angle of the geomagnetic field is $\theta_i = 10^\circ$. The total vertical distance of the simulation is L_z = 2000 km.

Our simulations have been demonstrated that for the quasi-electrostatic simulations when the inclination angle is $\theta_i > 10^\circ$, the distributions become smeared in the horizontal plane. This numerical effect does not change the results qualitatively; it can be removed accounting for the curvature of the geomagnetic field lines, using a curvilinear coordinate frame. Also, the tuning of the locally horizontal region of simulations in the upper ionosphere and the magnetosphere should be realized. But there is a simpler solution to the pointed above problem [46]. Since the longitudinal conductivity, that is, the component along the geomagnetic field line, is 5–7 orders of magnitude greater than the transverse conductivity in the upper ionosphere and magnetosphere, it is possible to make a connection by short-circuiting two regions of the ionosphere, namely the one from which the geomagnetic field line comes out and the one into which this line enters, i.e., magnetically conjugated region. Thus, the corresponding ionospheric regions located at altitudes up to z = 300 km can be connected. In other words, in the quasi-electrostatic simulations, it is possible to avoid the simulations within the upper ionosphere and the magnetosphere. Of course, this procedure is valid only in quasi-electrostatic simulations in the case of closed geomagnetic field lines. In this simplified approach the results of simulations are of agreement with the dynamic simulations under greater inclination angles $\theta_i > 20^\circ$. The results of simulations at higher inclination angles are given in Figures 11 and 12, the quasi-electrostatic and dynamic simulations correspondingly.

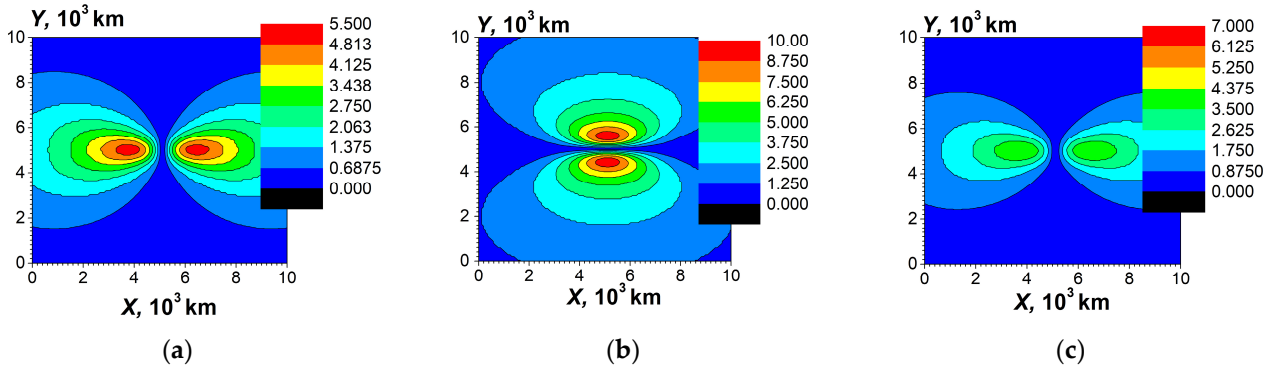

Figure 11. Distributions of the electric field components (in mV/m) in the ionosphere *F*-layer at the height z = 200 km. The quasi-electrostatic simulations, the case of closed geomagnetic field lines. The frequency is $\omega = 0.025\ s^{-1}$. It is increased inclination angle compared with Figure 8. Part (**a**) is $|E_x(x,y)|$, (**b**) is $|E_y(x,y)|$, (**c**) is $|E_z(x,y)|$. The geomagnetic field inclination is $\theta_i = 40^\circ$. The part of the higher ionosphere and the magnetosphere above 300 km has been eliminated by means of the short circuit along the geomagnetic field lines.

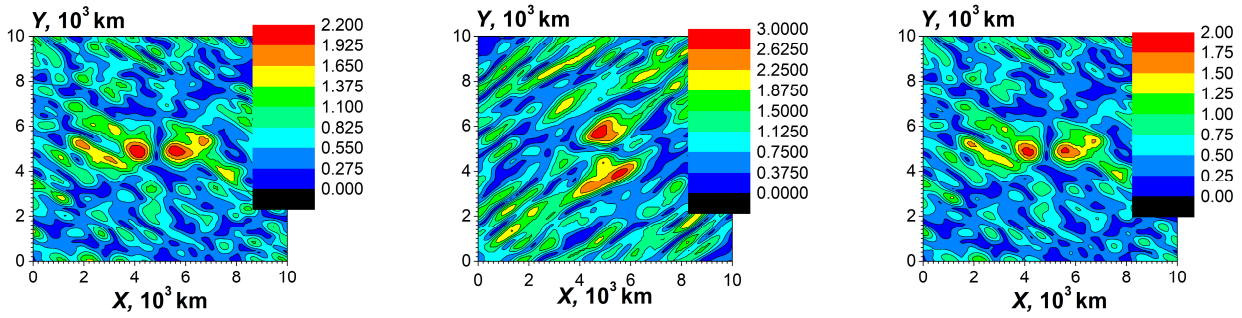

Figure 12. Distributions of the electric field components (in mV/m) in the ionosphere *F*-layer at the height z = 200 km. The dynamic simulations, the case of closed geomagnetic field lines. The frequency is $\omega = 0.025$ s^{-1}. Part (**a**) is $|E_x(x,y)|$, (**b**) is $|E_y(x,y)|$, (**c**) is $|E_z(x,y)|$. It is increased inclination angle compared with Figure 9, the inclination angle is $\theta_i = 40^\circ$. The total vertical distance of the simulation is L_z = 2000 km.

From Figures 11 and 12 it is seen that in the case of the closed geomagnetic field lines the correspondence between the values of the penetrated electric field obtained in the dynamic and quasi-static simulations is also valid at higher inclination angles of the geomagnetic field. The maximum values of $|E_y|$ component along the axis *OY* perpendicular to the geomagnetic field are practically the same in Figure 9e, and in Figure 12b, for the dynamic simulations; and in Figure 10b, and Figure 11b, for the quasi-static ones

From Figure 6, Figure 9, and Figure 12 it is seen that in the horizontal distributions $|E_{x,y,z}|(x,y)$ there exists the prolonged fine structure of the scales ~4000 km. This structure is more expressed at lower frequencies, compared to Figures 6 and 9, parts a, b, c at $\omega = 0.05$ s^{-1}, and parts d, e, f, $\omega = 0.025$ s^{-1}. The main maxima are similar for all frequencies. The origin of this fine structure is due to propagation of the EM waves in the gyrotropic ionosphere and in the lower magnetosphere, $z \leq 600$ km, which are strongly non-uniform in the vertical direction. The strong coupling between outgoing waves and backward ones occurs there. Such interference is more essential at lower frequencies where the longitudinal wave numbers are smaller. Our simulations have demonstrated that at higher frequencies $\omega > 0.05$ s^{-1} this prolonged structure is practically absent. The prolonged structures are less pronounced at inclination angle $\theta_i = 40^o$ (Figure 12a–c) than at $\theta_i = 10^\circ$ (Figure 9d–f). The details of forming this structure should be a subject of special investigations, especially at lower frequencies $\omega < 0.025$ s^{-1}.

At lower frequencies $\omega < 0.025$ s^{-1} the utilized algorithm for the dynamic simulations needs the extremely large amount of the computer memory, namely the decrease of the frequency two times demands the increase of the memory at least four times, i.e., the doubling of the points along both *OX* and *OY* axes. The reason is that the field components E_x, E_y are used as independent functions under the dynamic simulations and the transition to the exactly static case $\omega \to 0$ is a non-trivial computation problem. In the quasi-static simulations, the single function φ is used at all frequencies and the problem pointed above is absent.

The dependencies of the maximum values of the electric field components on the position of the external current have been simulated. A dynamic approach was used for the cases of open and closed field lines (see the first and second lines in Table 1). It is seen that the maximum values only slightly depend on the position of the maximum external current density when this current lies in the atmosphere, $z_1 \geq z_0$. Some decrease occurs when the current partially cuts of by the Earth's surface. Additionally, in Table 1 (see the third line) there are dependencies of the maximum values of the electric field components for the closed geomagnetic lines obtained under the quasi-electrostatic simulations.

Table 1. The dependencies of the maximum values of $|E_x|$, $|E_y|$, $|E_z|$, mV/m, on the position of the excitation current z_1, the circular frequency is $\omega = 0.025$ s^{-1}. The inclination angle of the geomagnetic field is $\theta_i = 10°$. There are the same parameters $z_0 = 7$ km, $j_0 = 0.1$ μA/m^2; $x_0 = y_0 = 500$ km, besides the data in the last column of the table.

z_1, km	14	10	7	5	3	0	0, but $x_0 = y_0 = 1000$ km
Dynamic simulations, open lines	1.7 2.0 0.3	1.65 2.0 0.29	1.6 1.85 0.28	1.45 1.7 0.255	1.25 1.5 0.22	0.85 1.0 0.15	1.55 1.62 0.275
Dynamic simulations, closed lines	2.45 2.8, 0.43	2.44 2.8 0.43	2.35 2.65 0.41	2.15 2.42 0.38	1.85 2.1 0.33	1.3 1.45 0.23	2.37 2.42 0.42
Quasi-electrostatic simulations, closed lines	3.6 7.3 0.50	2.5 5.1 0.35	1.8 3.6 0.25	1.36 2.7 0.19	0.96 1.93 0.13	0.5 0.99 0.07	0.92 2.0 0.13

Note that the dependence on the vertical coordinate in the spatial distribution of the external current (9) with the parameters $z_1 = (3–5)$ km, $z_0 = 7$ km corresponds qualitatively to the distribution of seismogenic external current in [67]; transverse scale $x_0 = y_0 = 500$ km and 1000 km correspond to the parameters of powerful earthquakes with magnitudes $M = 6.27$ and 6.98, respectively [68]. As it is seen from Table 1, electric field penetrating at a given altitude in the ionosphere with the chosen parameters differ less than 1.5 times, for the cases of open and closed geomagnetic field lines, in the simulations based on the dynamic approximation.

The distributions of the electric field components are presented for the case when the external current partially is cut by the Earth's surface, Figure 13.

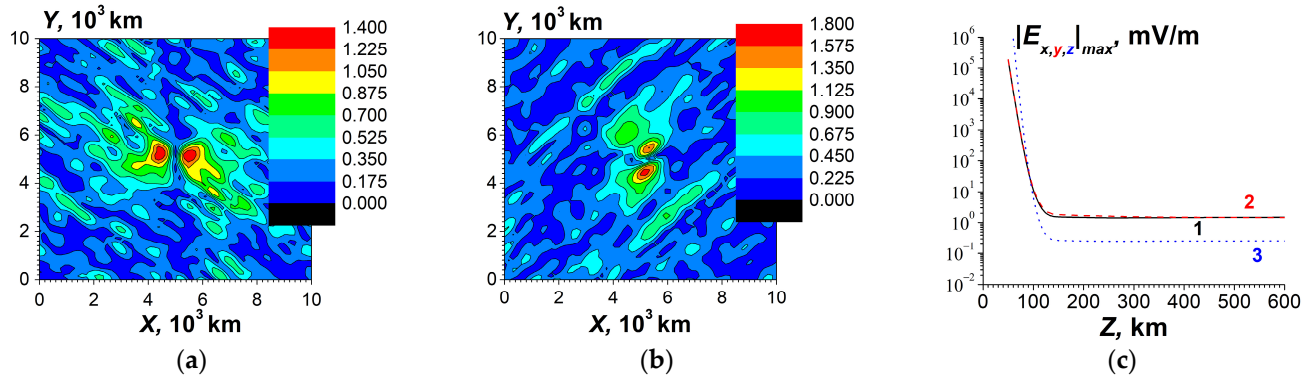

Figure 13. Distributions of the electric field components $|E_x|$, $|E_y|$ (in mV/m), parts (**a**,**b**), in the ionosphere *F*-layer at the height $z = 200$ km. The dynamic simulations. The case of open geomagnetic field lines is considered here. The frequency is $\omega = 0.025$ s^{-1}. The total vertical distance of the simulation is $L_z = 1500$ km. The geomagnetic field inclination is $\theta_i = 10°$. The parameters are $z_1 = 5$ km. $z_0 = 7$ km. In the part (**c**) the dependencies of the maximum values of the electric field components on z are presented, curve 1 is $|E_x|$, 2 is $|E_y|$, 3 is $|E_z|$.

It is seen that the distributions shown in Figure 13a,b are similar to ones in Figure 6d,e, respectively, while curves 1, 2, 3 in Figure 13c are similar to curves 3 in Figure 5a–c, respectively. The difference is in 15% smaller maximum values of $|E_x|$, $|E_y|$ in Figure 13, due to the cut-off of the external current by the Earth's surface.

In addition to the calculations, presented in Table 1, it was also shown that for the quasi-electrostatic case and closed geomagnetic field lines, in the frequency range 10^{-4} s^{-1} $\leq \omega \leq 0.025$ s^{-1}, the dependence of the maximum values of the electric field components on the frequency, at $z = 200$ km changes unessentially within 3% difference; this was shown, in particular, for the parameters $z_1 = 14$ km, $z_0 = 7$ km. Note also that, in the frequency range 10^{-4} s^{-1} $< \omega < 10^{-3}$ s^{-1}, the calculations are rather formal and mathematical in

nature. The reason is that during a time of order of the corresponding period of oscillations, $2\pi/\omega \sim 20$ h ($\omega \sim 10^{-4}$ s^{-1}), the changes in the parameters of the atmosphere and ionosphere, ignored in the frequency domain presentation, are already quite essential.

4. Discussion

The important problem of the penetration of the electric field to the ionosphere from the near-Earth sources is under investigation till now. A standard approach is the utilization of the electrostatic or quasi-electrostatic equation for the electric potential in media with highly anisotropic conductivity supplemented by boundary conditions. At the high conductive solid Earth's surface, the boundary condition is a constant value of the electric potential. Usually, some boundary condition for the electric potential and its derivatives is formulated at the boundary between the upper atmosphere and the lower ionosphere. But still, it has been unclear what boundary condition should be applied within the quasi-electrostatic approach in the magnetosphere and how to transfer the boundary condition to the lower ionosphere and whether such a transfer is valid. This basic problem is due to the high anisotropy of the conductivity of the upper ionosphere and the magnetosphere and mathematically is expressed through the product of a small value of the electric field along the geomagnetic field line and a very big value of the conductivity along with it, in order to calculate the density of the electric current. Thus, within the framework of the electrostatics, the correct formulation of the upper boundary condition for the electric potential is doubtful.

Nevertheless, the processes in the ionosphere and the magnetosphere are principally dynamic, so the case of the quasi-electrostatics may be justified only at small spatial scales. To perform this approximation, the condition (25) must be satisfied. The maximal period T can be estimated as $T \leq 2{\cdot}10^3$ s, i.e., the variation time of the current sources is smaller than 1 hour. Therefore, for the validity of the quasi-electrostatics, the distance along the geomagnetic field line should be $L_z < 2{\cdot}10^4$ km. From this simple estimation, it is seen that in the case of the open geomagnetic lines the quasi-electrostatic approximation is doubtful, whereas for the closed geomagnetic field lines it could be valid.

Generally, the dynamic approach should be used to consider the problem of penetration of the ULF electric field to the ionosphere. The simulations within the quasi-electrostatic approximation should correspond to the results of the dynamic simulations. The dynamic method is based on the Maxwell equations and proper boundary conditions for the electromagnetic field. Because the physical processes possess various temporal scales, to make the qualitative analysis as clear as possible, it is rather better to apply the spectral approach, i.e., within the frequency domain. Our dynamic simulations have been proven that in the case of open geomagnetic field lines the quasi-electrostatic approximation does not provide adequate results. Moreover, the results of simulations obtained within the dynamic method do not depend on the position of the upper boundary within the magnetosphere when the heights are $\geq$1000 km, which proves the validity of the dynamic approach. The boundary conditions for the EM field are the absence of the ingoing magnetohydrodynamic waves. Contrary to this, in the case of open geomagnetic lines, the results of the quasi-electrostatic simulations depend on the position of the upper boundary condition and the penetrated electric field in the ionosphere *F*-layer is several orders smaller than one obtained in the dynamic simulations.

In the case of the open geomagnetic field lines, the dynamic method for the penetration of the ULF electric fields from near-Earth sources to the upper ionosphere and magnetosphere is similar to the consideration of penetration of the magnetosphere perturbations due to the solar wind to the lower ionosphere and the atmosphere. Namely, those perturbations propagate along the magnetic field line as the magnetohydrodynamic waves, and only near the Earth's surface the quasi-static approximation is valid and used [69].

The physical reason for the significant difference between the results obtained on the basis of the dynamic and quasi-static approaches (Figures 5 and 7) in the case of open magnetic field lines is as follows. In the dynamic approach, we use the radiation condition

(Equations (11) or (12)) as the "upper boundary condition". This condition is set at the heights of the upper ionosphere or magnetosphere, where, for the frequency range under consideration, inhomogeneities in the medium are so smooth on the wavelength scale that the reflection for a wave emitted from the studied area can be neglected with sufficient accuracy [70]. This condition corresponds to the principle of causality [71], in particular, in the presence of (external current) sources only in the lower atmosphere. It turns out that the field excited by a given source in the lower atmosphere and penetrating into the ionosphere and magnetosphere is negligibly dependent on the location of the boundary at which the "upper boundary condition" (of radiation) is set in the upper ionosphere or magnetosphere (see Figure 5 and its description in Section 3). As for the quasi-static approach, it is applicable, if (25) is satisfied. Obviously, in the case of open geomagnetic field lines, a similar condition is violated at a sufficiently large value of L_z, for example, at L_z = 25,000 km. This is confirmed by the corresponding modeling illustrated in Figure 7.

In addition to this, we can also offer the following visual explanation of the significant difference between the results obtained on the basis of the dynamic and quasi-static approaches. If the radiation condition under the dynamic approach is formulated at a certain value of the coordinate $z = L_{z1}$, then we can assume that at $z > L_{z1}$ there are, respectively, only waves radiated from the considered region $0 \leq z \leq L_z$. If we now set the radiative boundary condition at $z = L_{z2} > L_{z1}$, then in both regions $L_{z1} < z \leq L_{z2}$, $z > L_{z2}$, in fact, only outgoing waves will be present, since the reflection in the region $L_{z1} < z \leq L_{z2}$ is negligible. Therefore, the field in the region $z < L_{z1}$, including the lower and middle ionosphere, will be practically insensitive to the location of the "upper boundary" selected in the upper ionosphere or magnetosphere (at $z = L_{z1}$ or $z = L_{z2}$). The situation is significantly different when the quasi-static approximation is used. In this approximation, there is neither delay nor radiation. As a result, when using the quasi-static approximation, the entire region $0 \leq z \leq L_z$ automatically belongs to the "region of influence" in the solution, even at very large values of L_z. Therefore, the value L_z, which determines the place where the "upper boundary condition" is specified, significantly affects the solution when applying the quasi-electrostatic approximation. This indicates the inapplicability of the quasi-electrostatic approximation in the case of open geomagnetic field lines.

In the case of the closed geomagnetic field lines both the dynamic approach and quasi-electrostatic one yield practically similar results for the penetration of the electric field into the ionosphere *F*-layer. Therefore, it is natural to set the appropriate boundary conditions on the surface of the Earth, in the regions from which the geomagnetic field lines emerge and where they return. Boundary conditions are set in a similar way when using the quasi-static approximation. Both in the quasi-electrostatics and in the dynamic approach the boundary conditions are zero values of the tangential electric field on the Earth surface; in the quasi-electrostatics, they are equivalent to the zero-electric potential.

It was mentioned in [46] the difference between the pointed above configurations of the geomagnetic field lines for the electrostatic simulations and the necessity to use different boundary conditions in the lower ionosphere. The upper boundary conditions used in [46,47] correspond qualitatively and by mathematical structure to the upper boundary condition derived in the present paper, see Appendix C, Equation (A53).

In Section 3 it has been mentioned the mathematical limitation for the lowest frequency that can be used in our model of the dynamic simulations. This mathematical limitation seems not occasional and has a physical sense with respect to an attempt to "move" into the region of lower frequencies on the basis of the dynamic approach. Namely, with decreasing frequency, one should expect that the solution for the electromagnetic field can be represented in terms of electromagnetic potentials [66,71,72]. Alternatively, such a solution can be presented in terms of magnetic and electrical Hertz potentials, which in the limit of low frequencies are transformed into electrostatic and magnetostatic potentials [71]. With this approach, it is quite obvious that the solution of the dynamic problem, in principle, cannot reach the purely electrostatic limit, since in this case "the magnetostatics is lost". In

any case, this must necessarily happen in the presence of low-frequency currents in the system, as in our case. In a geophysical experiment, this corresponds to the presence of a magnetic ULF field, excited by the corresponding currents, which can be measured at ground-based and satellite observatories.

Despite the fact that in this work a different approach is used with the reduction of Maxwell equations in the frequency domain to a system of two equations of the second order (8) for the Fourier amplitudes of two transverse components of the electric field, it seems obvious that also, in this case, two corresponding functions, associated with the transverse components of the electric field, cannot in the limit tend to a single function, namely, the electrostatic potential. The aforementioned mathematical difficulty with an increase in the required amount of RAM with a decrease in the source frequency is probably a mathematical reflection of the physical problem of the transition to quasi-electrostatics and quasi-magnetostatics. In the future, it will be of interest to consider the question of the "magneto-electrostatic" limit for the electrodynamic solution in the LEAIM system.

Our dynamic simulations, supplemented by quasi-electrostatic simulations (for the case of closed geomagnetic field lines) have demonstrated that the values of the electric field are, by the order of value, of about several, namely (1–5) mV/m in the lower ULF range of frequencies (10^{-3} s$^{-1} \leq \omega \leq 5 \cdot 10^{-2}$ s^{-1}) in the ionosphere *F*-layer at the heights z = 200–600 km and in the lower magnetosphere. Moreover, the corresponding simulations may be done even at such low frequencies, as 10^{-4} s$^{-1} \leq \omega < 10^{-3}$ s^{-1}, but only formally, if one would ignore the fact, that the parameters of the atmosphere and ionosphere change essentially during the period ($2\pi/\omega \sim$ 20hours, $\omega \sim 10^{-4}$ s^{-1}) of corresponding current source oscillations.

The results for the penetration of electric field into the ionosphere are obtained using the models of external current sources localized in the lower atmosphere with a maximum value of 0.1 μA/m^2, generated by tropical cyclones [54,56,57] or seismogenic (earthquake preparation) processes [1,6,24]. Such electric fields, by the order of value, are corresponding to the ionospheric observations above tropical hurricanes [61,73] and the region of the preparation of strong earthquakes [40]. Such values of the electric field correspond also to the observations of seismogenic variations in electron concentration and TEC [6,41]. Therefore, the simulated values of the electric field are of a qualitative agreement with the results of observations. Note also that the value of the extraneous current maximum of ~ 0.1 μA/m^2 accepted in the calculations in this work is far from the maximum possible corresponding value known from the literature. Namely, there are theoretical estimates that substantiate the possibility of generating external currents in the lower atmosphere with values exceeding those mentioned above by one or even two orders of magnitude. Such estimates are given, in particular, in works devoted to modeling and observations of ionospheric effects caused by electric fields from surface current sources of a seismogenic nature (during the preparation of powerful earthquakes) [6,67,74,75] and sources associated with tropical cyclones [54,56].

The external current only mimics the real current generated in the lower atmosphere by all physical processes taking place in a self-consistent manner, but at the same time, it allows one to determine the field penetrating into the upper ionosphere/magnetosphere. To adequately determine the electric field in the lower atmosphere, a synergetic approach is required with consideration of all relevant physical processes, instabilities in the LEAIM system, their nonlinear limitation [9,15,34], as well as the corresponding boundary conditions, including ones in the lower atmosphere, for various current components associated with different types of charged particles, including aerosols and ions, and taking into account photochemistry, convection, hydration and other dynamic processes [1,4,6,24,32]. The synergetic approach would include, naturally, the self-consistent investigations with accounting for positive feedback between the penetrated EM field and changes in the ionosphere parameters. This may be a subject of future works.

5. Conclusions

The penetration of an electric field through the LEAIM system is of a dynamic nature, in particular, in the presence of external current sources exciting the electromagnetic fields in the lower atmosphere or lithosphere. This dynamic nature is due to the variation in time in both properties of the atmosphere, ionosphere, and the magnetosphere and of the external sources. Also, it should be taken into account the possible propagation of electromagnetic disturbances over large distances along the geomagnetic field lines. This propagation results in retardation of the electromagnetic field. Thus, the correct formulation of the problem should be done, generally speaking, on the basis of a dynamic approach to solving the Maxwell equations.

In this case, the corresponding dynamic boundary conditions for the electromagnetic field must also be formulated correctly. The ULF waves considered in this paper propagate to a large distance along the lines of the geomagnetic field. Two essentially different situations arise: (1) the geomagnetic field lines emerging from the Earth-Atmosphere boundary in the region of the location of an external electric current source are open, passing from the upper ionosphere into the deep magnetosphere, and do not return into the ionosphere (for sufficiently high latitudes); (2) after penetration from the ionosphere into the lower magnetosphere, the geomagnetic field lines return to the magnetically conjugated ionosphere and then again fall from the atmosphere into the Earth (lithosphere). Naturally, for the electromagnetic field at the "second end" of the line of force, where the numerical calculation completes, there are significantly different boundary conditions. In the case of open field lines, this is the condition of radiation, and in the case of closed field lines, the tangential component of the electric field is equal to zero, if the conductivity of the Earth is considered equal to infinity. It turns out that in the case of open geomagnetic field lines only the dynamic approach is applicable, but the quasi-static approach is not valid, and in the case of closed geomagnetic field lines the quasi-static approximation can also be used, since it gives results that qualitatively and quantitatively, by the order of value, coincide with the results obtained on the base of the dynamic approach. In the case of closed filed lines, the electric potential calculated in the upper part of the first ionosphere (located above the region where external sources are considered) can be transferred along the geomagnetic field lines to the upper part of the magnetically conjugated ionosphere, and then it will continue the calculation, in particular, in the atmosphere magnetically conjugated region.

The values of the electric field obtained in the dynamic approximation are of about several (1–5) mV/m in the ionosphere *F*-layer and in the lower magnetosphere. In this case, the results are similar to ones obtained within the quasi-electrostatic approximation simulations when the geomagnetic field lines return to the Earth's surface. In the region near the boundary between the atmosphere and the ionosphere $z = 60$ km the electric fields are several (1–5) V/m. The external electric current sources have a maximum value of 0.1 $\mu A/m^2$ and are localized in the lower atmosphere. The simulated values of the electric field are of a qualitative and even quantitative, by the order of value, agreements with the results of observations of electric fields and perturbations of the electron concentration/TEC, caused by the current developed in connection with tropical cyclones or the seismogenic processes (the preparation of the most powerful earthquakes).

Note that to the parameters used for the modeling presented in Figures 5 and 6, the estimation (24) of the penetration depth appeared to be suitable and corresponds qualitatively to the results presented in the Figures mentioned above.

Numerical-analytical algorithms are given in detail, including the derivation of boundary conditions and a numerical scheme based on a combined spectral–finite difference method for dynamically modeling the field penetration from a given electric current sources in the lower atmosphere through the LEAIM system.

Author Contributions: Conceptualization, methodology, V.Y., Y.R., V.G.,V.I.; software, data curation V.G., A.G., A.F.; validation, Y.R., A.G., S.P.; investigation, Y.R., V.I.; writing—original draft preparation, Y.R., V.G., A.G., V.I.; writing—review and editing, V.Y., S.P., A.F., V.K.; discussion, interpretation of physical results and conclusions, all authors; visualization (preparation of figures), Y.R., S.P., V.K.; supervision, V.Y.,Y.R.; project administration, Y.R., A.G. All authors have read and agreed to the published version of the manuscript.

Funding: Financial support for this research was partially provided by CONACYT-Fondos Sectoriales grant CONACYT project A1-S-29604 to Vsevolod Yutsis. Yuriy Rapoport, Asen Grytsai, Vasyl Ivchenko, Sergei Petrishchevskii and Valery Krivodubskij are thankful to the Ministry of Education and Science of Ukraine for the partial support of the present work, grant 20BF051-02 [0120U102178] "Wave processes and effects in active resonant layered plasma media and metamaterials". Alla Fedorenko is thankful to the National Research Foundation of Ukraine for the support of the work by grant 2020.02/0015 "Theoretical and experimental studies global perturbations of natural and artificial origin in the Earth-atmosphere system".

Institutional Review Board Statement: Not applicable.

Informed Consent Statement: Not applicable.

Data Availability Statement: The corresponding ionospheric data have been taken from the well-known published handbooks, referred in the paper [18,51,52,63–65]. There is implementation of the standard and approbated computed code without using the commercial software. The computer codes are the finite difference schemes, the Fast Fourier transform, the matrix factorization method, the correct approximation of the boundary conditions for different cases. The description of the computer codes is presented in the text of the paper in Appendices B and C, as well as in proper references [48–50].

Conflicts of Interest: The authors declare no conflict of interest.

Appendix A. Details of the Derivation of the Dynamic Equation

For the case when the frequency of the electromagnetic wave is not zero, the expression for the conductivity tensor in the magnetized ionospheric plasma, which corresponds to the values of the components of the dielectric constant, is obtained from (2)–(5). Let's move on to deriving the dynamic equation. Consider the electromagnetic field excited by an external current in the LEAIM system.

Since the parameters of the medium are considered to depend only on the vertical coordinate z, the spectrum of electromagnetic fields excited by the source $\vec{J}^{ext}$ is discrete with horizontal wave numbers (k_x, k_y) and the amplitude of the Fourier components, which depends on z. The corresponding Fourier decompositions for electric and magnetic fields have the form

$$E_{x,y,z} = \sum_{k_x,k_y} e^{i(\omega t - k_x x - k_y y)} E_{x,y,z}^{(k_x,k_y)}(z), \tag{A1}$$

$$H_{x,y,z} = \sum_{k_x,k_y} e^{i(\omega t - k_x x - k_y y)} H_{x,y,z}^{(k_x,k_y)}(z). \tag{A2}$$

An external current source can be represented in the form

$$J_{x,y,z} = \sum_{k_x,k_y} e^{i(\omega t - k_x x - k_y y)} j_{x,y,z}^{(k_x,k_y)}(z). \tag{A3}$$

In the relations (A1)–(A3), $E_{x,y,z}^{(k_x,k_y)}(z)$, $H_{x,y,z}^{(k_x,k_y)}(z)$, $J_{x,y,z}^{(k_x,k_y)}(z)$ are the Fourier amplitudes of the corresponding quantities. The Maxwell equations can be written in the form

$$\vec{\nabla} \times \vec{H} = ik_0 \vec{D} + \frac{4\pi}{c} \vec{j};\ k_0 \equiv \frac{\omega}{c};\ \vec{D} = \hat{\varepsilon} \vec{E}, \tag{A4}$$

$$\vec{\nabla} \times \vec{E} = -ik_0 \vec{H}. \tag{A5}$$

When developing the algorithm, we take into account that the elements of the tensor $\hat{\varepsilon}$ (see relation (5)) depend on the vertical coordinate z, namely:

$$\hat{\varepsilon} = \begin{pmatrix} \varepsilon_{11}(z) & \varepsilon_{12}(z) & \varepsilon_{13}(z) \\ \varepsilon_{21}(z) & \varepsilon_{22}(z) & \varepsilon_{23}(z) \\ \varepsilon_{31}(z) & \varepsilon_{32}(z) & \varepsilon_{33}(z) \end{pmatrix} \equiv \hat{\varepsilon}(\omega, z). \tag{A6}$$

Using (A4), (A5), we obtain:

$$\begin{gathered} \vec{\nabla} \times \vec{\nabla} \times \vec{E} = -ik_0 \vec{\nabla} \times \vec{H} = -ik_0 \left(ik_0 \vec{D} + \tfrac{4\pi}{c} \vec{j} \right) = k_0^2 \vec{D} - \tfrac{4\pi i k_0}{c} \vec{j}, \\ -\vec{\nabla} div \vec{E} + \Delta \vec{E} + k_0^2 \vec{D} - \tfrac{4\pi i k_0}{c} \vec{j} = 0. \end{gathered} \tag{A7}$$

Below, we use the combined spectral-difference method [48–50]. Namely, we perform the Fourier transform of Equation (A7), taking into account (A6). As a result, we obtain the ratios for the Fourier components of the fields included in (A1)–(A3). Writing the corresponding equation for the Fourier components, we omit, as already noted, the subscripts (k_x, k_y). The same applies to the Fourier component of an external source $\vec{J}^{ext}$. All Fourier amplitudes depend on z, as can be seen from (A1)–(A3). Having written formulas for the Fourier components of fields and currents below, we omit the dependences on z, using the notations $E_x^{(k_x,k_y)}(z) \to E_x$, $J_x^{(k_x k_y)}(z) \to J_x$.

In the variables x, y, z Equation (A7) takes the form:

$$(x) \frac{\partial^2 E_x}{\partial z^2} - k_y^2 E_x + k_x k_y E_y + ik_x \frac{\partial E_z}{\partial z} + k_0^2 D_x - \frac{4\pi i k_0}{c} J_x = 0, \tag{A8}$$

$$(y) \frac{\partial^2 E_y}{\partial z^2} - k_x^2 E_y + k_x k_y E_x + ik_y \frac{\partial E_z}{\partial z} + k_0^2 D_y - \frac{4\pi i k_0}{c} J_y = 0, \tag{A9}$$

$$(z) - (k_x^2 + k_y^2) E_z + k_0^2 D_z + ik_x \frac{\partial E_x}{\partial z} + ik_y \frac{\partial E_y}{\partial z} - \frac{4\pi i k_0}{c} J_z = 0. \tag{A10}$$

By marking $k_t^2 \equiv k_x^2 + k_y^2$ and using (A10), one can get

$$\begin{gathered} E_z = -\Big(\tfrac{ik_x}{k_0^2} \tfrac{1}{\varepsilon_{33} - \frac{k_t^2}{k_0^2}} \tfrac{\partial E_x}{\partial z} + \tfrac{ik_y}{k_0^2} \tfrac{1}{\varepsilon_{33} - \frac{k_t^2}{k_0^2}} \tfrac{\partial E_y}{\partial z} \\ + \tfrac{\varepsilon_{33} E_x}{\varepsilon_{33} - \frac{k_t^2}{k_0^2}} + \tfrac{\varepsilon_{32} E_y}{\varepsilon_{33} - \frac{k_t^2}{k_0^2}} - \tfrac{\frac{4\pi i}{\omega} J_z}{\varepsilon_{33} - \frac{k_t^2}{k_0^2}} \Big). \end{gathered} \tag{A11}$$

By entering (A11) in (A8) and (A9) and denoting $\varepsilon_{33t} \equiv \varepsilon_{33} - k_t^2/k_0^2$, one can get a system of Equation (8) similarly to [15] with the corresponding coefficients in the form:

$$\hat{A}_1 = \frac{1}{\varepsilon_{33t}} \begin{bmatrix} \varepsilon_{33} - k_y^2/k_0^2 & \frac{k_x k_y}{k_0^2} \\ \frac{k_x k_y}{k_0^2} & \varepsilon_{33} - k_x^2/k_0^2 \end{bmatrix}, \tag{A12}$$

$$\hat{B}_{01} = -\begin{bmatrix} ik_x \frac{\varepsilon_{31}}{\varepsilon_{33t}} & ik_x \frac{\varepsilon_{32}}{\varepsilon_{33t}} \\ ik_y \frac{\varepsilon_{31}}{\varepsilon_{33t}} & ik_y \frac{\varepsilon_{32}}{\varepsilon_{33t}} \end{bmatrix}, \tag{A13}$$

$$\hat{B}_{02} = -\begin{bmatrix} ik_x \frac{\varepsilon_{13}}{\varepsilon_{33t}} & ik_y \frac{\varepsilon_{13}}{\varepsilon_{33t}} \\ ik_x \frac{\varepsilon_{23}}{\varepsilon_{33t}} & ik_y \frac{\varepsilon_{23}}{\varepsilon_{33t}} \end{bmatrix}, \tag{A14}$$

$$\hat{B}_F = \begin{bmatrix} \left[k_0^2 \left(\varepsilon_{11} - \frac{\varepsilon_{13}\varepsilon_{31}}{\varepsilon_{33t}} \right) - k_y^2 \right] & \left[k_0^2 \left(\varepsilon_{12} - \frac{\varepsilon_{13}\varepsilon_{32}}{\varepsilon_{33t}} \right) + k_x k_y \right] \\ \left[k_0^2 \left(\varepsilon_{21} - \frac{\varepsilon_{23}\varepsilon_{31}}{\varepsilon_{33t}} \right) + k_x k_y \right] & \left[k_0^2 \left(\varepsilon_{22} - \frac{\varepsilon_{23}\varepsilon_{32}}{\varepsilon_{33t}} \right) - k_x^2 \right] \end{bmatrix}, \tag{A15}$$

$$\vec{B}_{1J_z} = -\frac{4\pi}{\omega}\vec{k}_{tg},\ \vec{k}_{tg} \equiv (k_x, k_y)^T,\ \vec{e}_F = (e_x, e_y)^T, \tag{A16}$$

$$\hat{B}_{2J_z} = \frac{4\pi i k_0^2}{\omega \varepsilon_{33t}} \begin{bmatrix} \varepsilon_{13} & 0 \\ 0 & \varepsilon_{23} \end{bmatrix}. \tag{A17}$$

The relations (A12)–(A17) completely determine the coefficients of the matrix equation (8). Assume that (a) the medium above the upper boundary $z = L_z$ is a homogeneous anisotropic but not gyrotropic layer F [52] with parameters that do not depend on z; this is justified by the fact, that the parameters in the upper ionosphere and magnetosphere change much slower than in E region of the ionosphere [15]; (b) there are no sources of ULF waves in the region $z \geq L_z$. Therefore the plane (outgoing) waves propagate in the region $z \geq L_z$ in the positive direction of axis Z, and it is possible to find the connection between $\partial E_{x,y}/\partial z$ and $E_{x,y}$ at $z = L_z + \delta$, where δ is infinitesimally small positive value. Therefore accounting for that $E_{x,y}$ are continuous at $z = L_z$, we need to find the relationship between the derivatives $\partial E_{x,y}/\partial z$ at $z = L_z - \delta$ and $z = L_z + \delta$.

Tensor $\hat{\varepsilon}$ in the F layer of the ionosphere in the coordinate frame $x'y'z'$ has the following form [51,52]:

$$\hat{\varepsilon} = \begin{pmatrix} \varepsilon_1 & 0 & 0 \\ 0 & \varepsilon_1 & 0 \\ 0 & 0 & \varepsilon_3 \end{pmatrix}. \tag{A18}$$

Let us use for the ULF waves in F region the approximation

$$\varepsilon_3 \to \infty,\ E_z' \to 0 \tag{A19}$$

and account for that the following relationships for the vector components in the coordinate frames denoted with and without the primes (Figure 1):

$$\begin{aligned} k_x' &= k_x \cos\theta + k_z \sin\theta \\ k_z' &= -k_x \sin\theta + k_z \cos\theta \\ E_z' &= E_z \cos\theta - E_x \sin\theta \approx 0 \\ E_x' &= E_x \cos\theta + E_z \sin\theta \approx E_x / \cos\theta. \end{aligned} \tag{A20}$$

In accordance with Equation (A7), in the region $z \geq L_z$ with $\vec{J} = 0$, the following relations are valid:

$$\begin{aligned} &-\vec{\nabla} div\vec{E} + \Delta\vec{E} + k_0^2\vec{D} = 0 \\ &div\vec{D} = 0 \end{aligned} \tag{A21}$$

Put, for the region $z \geq L_z$

$$E_{x,y,z} = E_{x_0 y_0 z_0} e^{i(\omega t - \vec{k}'\vec{r}')} = E_{x_0 y_0 z_0} e^{i(\omega t - \vec{k}\vec{r})}. \tag{A22}$$

In Equation (A22), $E_{x_0 y_0 z_0}$ are complex amplitudes of the electric field components E_{xyz},

$$\vec{k}' \cdot \vec{r}' \equiv k_{x'}x' + k_{y'}y' + k_{z'}z' = \vec{k} \cdot \vec{r} \equiv k_x x + k_y y + k_z z. \tag{A23}$$

In Equation (A23), $\vec{r}$ and $\vec{r}'$ are the radius vectors in the systems xyz and $x'y'z'$, respectively, $\vec{k}' \equiv (k_x', k_y', k_z')$ is the wave vector in the system, where coordinates are denoted with primes (Figure 1). Accounting for (A20), (A23), Equation (A21) in the system $x'y'z'$ takes the form

$$\vec{k}'(\vec{k}'\vec{E}') - k'^2\vec{E}' + k_0^2\vec{D}' = 0, \tag{A24}$$

$$\vec{k}'\vec{D}' = 0. \tag{A25}$$

Equation (A24) can be presented in the form

$$k_{x'}(k_{y'}E_{y'} + k_{z'}E_{z'}) + (k_0^2\varepsilon_1 - k_{y'}^2 - k_{z'}^2)E_{x'} = 0, \tag{A26}$$

$$k_{y'}(k_{y'}E_{y'} + k_{z'}E_{z'}) + (k_0^2\varepsilon_1 - k_{x'}^2 - k_{z'}^2)E_{y'} = 0. \tag{A27}$$

In the approximation (A19), the following dispersion equation follows from (A26), (A27):

$$(k_0^2\varepsilon_1 - k'^2)(k_0^2\varepsilon_1 - k_{z'}^2) = 0;\ k'^2 = k_{x'}^2 + k_{y'}^2 + k_{z'}^2. \tag{A28}$$

According to Equation (A28), the dispersion equations for the ULF modes in cold plasma are:

$$\text{for Alfven waves (AW)}:\ k_{z'} = \pm k_0\sqrt{\varepsilon_1}; k_z \equiv k_a = k_x\tan\theta \pm \frac{k_0\sqrt{\varepsilon_1}}{\cos\theta}; \tag{A29}$$

$$\text{for fast magnetosonic waves (FMSW)}:\ k_z \equiv k_s = \pm\sqrt{\varepsilon_1 k_0^2 - k_x^2 - k_y^2}. \tag{A30}$$

Accounting for Equations (A26)–(A30), the following polarization relations are obtain

$$\text{for AW}:\ E_{y'} = E_y = \alpha_a E_x;\ \alpha_a = \frac{k_y}{k_x + k_a\sin\theta}; \tag{A31}$$

$$\text{for FMSW}:\ E_x = -\beta_s E_y;\ \beta_s = \frac{k_y\cos\theta}{k_x\cos\theta + k_s\sin\theta}. \tag{A32}$$

Note that, in accordance with Maxwell equations, accounting for (A20), (A22),

$$H_x \sim \frac{\partial E_z}{\partial y} - \frac{\partial E_y}{\partial z} = -ik_y E_z - \frac{\partial E_y}{\partial z} = -ik_y E_x\tan\theta - \frac{\partial E_y}{\partial z}, \tag{A33}$$

$$H_y \sim \frac{\partial E_x}{\partial z} - \frac{\partial E_z}{\partial x} = \frac{\partial E_x}{\partial z} + ik_x E_z = \frac{\partial E_x}{\partial z} + ik_x E_x\tan\theta. \tag{A34}$$

Accounting for (A34), (A35) and the continuity of $H_{x,y}, E_x$, one can conclude that derivatives $\partial E_{x,y}/\partial z$ are continuous at $z = L_z$, as well. Then to find the elements m_{ij}, $i, j = 1, 2$ (see relations (11), (12)), present the components $E_{x,y}$ of the ULF waves in the region $z \geq L_z$, accounting for (A29)–(A34), in the form:

$$\begin{array}{l} E_x = E_a e^{-ik_a\overline{z}} + \beta_s E_s e^{-ik_s\overline{z}} \\ E_y = \alpha_a E_a e^{-ik_a\overline{z}} + E_s e^{-ik_s\overline{z}} \\ \overline{z} = z - L_z;\ \mathrm{Im}(k_a) < 0;\ \mathrm{Im}(k_s) < 0 \end{array} \tag{A35}$$

In Equation (A35), $E_{a,s}$ are the corresponding complex amplitudes. Accounting for (A37), one can get for $z = L_z + \delta;\ \delta \to 0$

$$\begin{array}{l} E_x = E_a + \beta_s E_s \\ E_y = \alpha_a E_a + E_s \end{array} \tag{A36}$$

$$\begin{array}{l} \frac{\partial E_x}{\partial z} = -i(k_a E_a + \beta_s k_s E_s) \\ \frac{\partial E_y}{\partial z} = -i(k_a\alpha_a E_a + k_s E_s) \end{array} \tag{A37}$$

Excluding the amplitudes $E_{a,s}$ from the Equation (A36), one can obtain, using (A37) and the continuity of $E_{x,y}$, $\partial E_{x,y}/\partial z$ at $z = L_z$, the boundary conditions (11), (12) at $z = L_z - \delta$, $\delta \to 0$ with the coefficients

$$\begin{array}{l} m_{11} = \frac{i}{\Delta}(k_a - \alpha_s\beta_s k_s);\ m_{12} = \frac{i\beta_s}{\Delta}(k_s - k_a); \\ m_{21} = \frac{i\alpha_a}{\Delta}(k_a - k_s);\ m_{22} = \frac{i}{\Delta}(k_s - \alpha_a\beta_s k_a); \\ \Delta = 1 - \beta_s\alpha_a;\ \mathrm{Im}(k_a) < 0;\ \mathrm{Im}(k_s) < 0. \end{array} \tag{A38}$$

Then, one needs to solve the system of Equation (8) with matrix coefficients (A12)-(A17) and corresponding boundary conditions (11), (12) with coefficients (A38). This solution is performed using the numerical matrix run method [48,49].

At $z = 0$ (on the boundary Lithosphere/Earth-Atmosphere) either infinite Lithosphere/Earth conductivity with zero boundary conditions for $E_{x,y}$ are supposed or finite conductivity is accounted for; in the last case, zero boundary conditions are used inside the Lithosphere, in particular at the altitude $z = -30$ km.

Appendix B. Numerical Method for Solution of the System of Equation (8)

Numerical scheme based on the method of vector run [48–50] to solve the system of Equation (8) with boundary conditions (11), (12), as well as zero conditions for the x- and y-components of the electric field on the side walls (see Figure 1) and the lower boundary ($z = 0$) is presented.

Equations for the transverse components of the electric field have been approximated by the finite differences:

$$\begin{array}{l}\frac{1}{h_z{}^2}(\hat{A}_{1,j+1/2}\cdot(\vec{F}_{j+1}-\vec{F}_j)-\hat{A}_{1,j-1/2}\cdot(\vec{F}_j-\vec{F}_{j-1}))+\frac{1}{2h_z}(\hat{B}_{01,j+1}\cdot\vec{F}_{j+1}-\hat{B}_{01,j-1}\cdot\vec{F}_{j-1})\\ +\frac{1}{2h_z}\hat{B}_{02,j}\cdot(\vec{F}_{j+1}-\vec{F}_{j-1})+\hat{B}_{F,j}\cdot\vec{F}_j\\ +\frac{1}{2h_z}(\frac{1}{\varepsilon_{33t,j+1}}J^{ext}_{z,j+1}-\frac{1}{\varepsilon_{33t,j-1}}J^{ext}_{z,j-1})\cdot\vec{B}_{1J_z,j}\\ +\hat{B}_{2J_z,j}\cdot J^{ext}_{z,j}\cdot\vec{e}_F+B_{J_{tg},j}\cdot\vec{J}_{tg,j}=0;\\ or:\ \hat{\alpha}_{-1}\cdot\vec{F}_{j-1}+\hat{\alpha}_0\cdot\vec{F}_j+\hat{\alpha}_{+1}\cdot\vec{F}_{j+1}=\vec{f}_j;\ j=1,\ldots,N-1;\\ z_j\equiv h_z\cdot j,\ z_N\equiv L_z.\end{array} \tag{A39}$$

Here h_z is the step of discreteness along OZ axis. The expressions for the matrix coefficients and for $\vec{f}_j$ are

$$\begin{array}{l}\hat{\alpha}_{-1}=\frac{1}{h_z{}^2}\hat{A}_{1,j-1/2}-\frac{1}{2h_z}\hat{B}_{01,j-1}-\frac{1}{2h_z}\hat{B}_{02,j};\\ \hat{\alpha}_0=-\frac{1}{h_z{}^2}(\hat{A}_{1,j+1/2}+\hat{A}_{1,j-1/2})+\hat{B}_{F,j};\\ \hat{\alpha}_{+1}=\frac{1}{h_z{}^2}\hat{A}_{1,j+1/2}+\frac{1}{2h_z}\hat{B}_{01,j+1}+\frac{1}{2h_z}\hat{B}_{02,j};\\ \vec{f}_j=-\frac{1}{2h_z}((\frac{1}{\varepsilon_{33t}}J_z{}^{ext})_{j+1}-(\frac{1}{\varepsilon_{33t}}J_z{}^{ext})_{j-1})\vec{B}_{1J_z,j}-(J_z{}^{ext}\hat{B}_{2J_z})_j\vec{e}_F-(B_{J_{tg}}\cdot\vec{J}_{tg})_j.\end{array} \tag{A40}$$

The expressions are given for the constant step h_z, but also the variable step can be applied.

In the matrix factorization method the following expressions are used:

$$\vec{F}_j=\hat{\beta}_j\cdot\vec{F}_{j-1}+\vec{r}_j,\ j=N,\ldots,1. \tag{A41}$$

At the upper boundary in the magnetosphere the boundary conditions are, Equations (11) and (12)

$$\frac{d\vec{F}}{dz}+\hat{m}\cdot\vec{F}=0. \tag{A42}$$

So after the difference approximation they are rewritten as ($j = N$):

$$\frac{\vec{F}_N-\vec{F}_{N-1}}{h_z}+\hat{m}\cdot\vec{F}_N=0. \tag{A43}$$

Thus,

$$\begin{array}{l}\vec{F}_N=(\hat{I}+h_z\hat{m})^{-1}\cdot\vec{F}_{N-1},\\ or\ \hat{\beta}_N=(\hat{I}+h_z\hat{m})^{-1},\ \vec{r}_N=0.\end{array} \tag{A44}$$

In the case of closed filed lines, when the boundary conditions are at the Earth's surface, they are:

$$\hat{\beta}_N = 0,\ \vec{r}_N = 0. \tag{A45}$$

At $j = N - 1, \ldots, 1$ Equation (A39) may be rewritten as, once $\hat{\beta}_{j+1},\ \vec{r}_{j+1}$ are already known:

$$\begin{array}{l} \hat{M} \cdot \vec{F}_j = \vec{f}_j - \hat{\alpha}_{+1} \cdot \vec{r}_{j+1} - \hat{\alpha}_{-1} \cdot \vec{F}_{j-1};\ j = N-1, \ldots, 1; \\ where\ \hat{M} \equiv \hat{\alpha}_0 + \hat{\alpha}_{+1} \cdot \hat{\beta}_{j+1}. \end{array} \tag{A46}$$

Therefore, one can write down

$$\hat{\beta}_j = -\hat{M}^{-1} \cdot \hat{\alpha}_{-1},\ \vec{r}_j = \hat{M}^{-1} \cdot (\vec{f}_j - \hat{\alpha}_{+1} \cdot \vec{r}_{j+1});\ j = N-1, \ldots, 1. \tag{A47}$$

At the first Earth's surface the boundary condition is

$$\vec{F}_0 = 0,\ j = 0. \tag{A48}$$

And, once all the factorization coefficients $\hat{\beta}_j,\ \vec{r}_j;\ j = N, \ldots, 1$ are already known, one can compute the transverse components of the electric field $\vec{F}_j,\ j = 1, \ldots, N$ sequentially from (A41), as well as all another electromagnetic components.

The results of simulations do not depend on the step along *OZ* axis when this step is quite small, as usually $h_z < 1$ km.

Appendix C. Numerical Scheme for Quasi-Electrostatic Problem and Effective Boundary Condition

For the quasi-electrostatic simulations the algorithm is similar to one presented in Appendix A, but it is simpler and based on the ordinary factorization method with 3-diagonal matrices. The set of equations for the potential which follows from the system (6) has the structure:

$$\alpha_{-1} \cdot \varphi_{j-1} + \alpha_0 \cdot \varphi_j + \alpha_{+1} \cdot \varphi_{j+1} = f_j;\ j = 1, \ldots, N-1; \tag{A49}$$

In the case of the closed geomagnetic field lines the boundary conditions are at the Earth's surface: $\varphi = 0$. In the case of the open lines far from the Earth's surface the boundary condition is $E_z \equiv \partial\varphi/\partial z = 0$.

We suppose that the sources are absent within the interval from the point of the upper boundary conditions down till the boundary $z = z_c$ between the upper atmosphere and the lower ionosphere, Figure 3, $z_c < z < L_z$, $z_c = M \cdot h_z$, so, to solve the system (A49), it is possible to write down the following factorization formula:

$$\begin{array}{l} \varphi_j = \beta_j \cdot \varphi_{j-1},\ j = N, \ldots, M; \\ for\ closed\ lines\ \beta_N = 0; \\ for\ open\ lines\ \beta_N = 1. \end{array} \tag{A50}$$

Here the absence of the source currents in the region $z_c < z < L_z$ is taken into account. Note that the second and third relations from (A50) correspond to the boundary conditions $\varphi = 0$ and $\partial\varphi/\partial z = 0$, respectively, at $z = L_z$. At $z = z_c$, accounting for the first relation from (A50), it is possible to write down:

$$\frac{\partial\varphi(k_x,k_y)}{\partial z}|_{z=z_c} \approx \frac{\varphi_M - \varphi_{M-1}}{h_z} = \frac{\beta_M - 1}{h_z}\varphi_{M-1}(k_x,k_y) \equiv Q(k_x,k_y) \cdot \varphi_{M-1}(k_x,k_y). \tag{A51}$$

The Equation $\varphi = 0$(A51) is the boundary condition transferred from $z = L_z$ to the point $z = z_c$. In the spatial representation Equation (A51) can be rewritten as:

$$\begin{array}{l} \frac{\partial\varphi(x,y)}{\partial z} \approx Q(0,0)\cdot\varphi(x,y) + i\left(\frac{\partial Q}{\partial k_x}\frac{\partial\varphi}{\partial x} + \frac{\partial Q}{\partial k_y}\frac{\partial\varphi}{\partial y}\right) \\ -\frac{1}{2}\left(\frac{\partial^2 Q}{\partial k_x^2}\frac{\partial^2\varphi}{\partial x^2} + \frac{\partial^2 Q}{\partial k_y^2}\frac{\partial^2\varphi}{\partial y^2} + 2\frac{\partial^2 Q}{\partial k_x \partial k_y}\frac{\partial^2\varphi}{\partial x\partial y}\right). \end{array} \quad \text{(A52)}$$

This is the transfer of the upper boundary condition to the boundary point between the upper atmosphere and the lower ionosphere. Numerical computation shows that the first and second terms in the right-hand side of Equation (A52) are rather small. Therefore Equation (A52) can be approximately presented in the form

$$\frac{\partial\varphi(x,y)}{\partial z} + \frac{1}{2}\left(\frac{\partial^2 Q}{\partial k_x^2}\frac{\partial^2\varphi}{\partial x^2} + \frac{\partial^2 Q}{\partial k_y^2}\frac{\partial^2\varphi}{\partial y^2} + 2\frac{\partial^2 Q}{\partial k_x \partial k_y}\frac{\partial^2\varphi}{\partial x\partial y}\right) = 0 \quad \text{(A53)}$$

These boundary conditions (A52), (A53) correspond qualitatively and by mathematical structure to the upper boundary condition presented, in particular, in Denisenko et al. (2008) [47], see Equation (14) and Figure 1 in that paper.

References

1. Sorokin, V.M.; Chmyrev, V.M.; Hayakawa, M. A Review on Electrodynamic Influence of Atmospheric Processes to the Ionosphere. *Open J. Earthq. Res.* **2020**, *9*, 113–141. [CrossRef]
2. Pulinets, S.A.; Davidenko, D.V. The Nocturnal Positive Ionospheric Anomaly of Electron Density as a Short-Term Earthquake Precursor and the Possible Physical Mechanism of Its Formation. *Geomagn. Aeron.* **2018**, *58*, 559–570. [CrossRef]
3. Guo, J.; Li, W.; Yu, H.; Liu, Z.; Zhao, C.; Kong, Q. Impending ionospheric anomaly preceding the Iquique Mw8.2 earthquake in Chile on 2014 April 1. *Geophys. J. Int.* **2015**, *203*, 1461–1470. [CrossRef]
4. Grimalsky, V.; Hayakawa, M.; Ivchenko, V.; Rapoport, Y.; Zadorozhnii, V. Penetration of an electrostatic field from the lithosphere into the ionosphere and its effect on the D-region before earthquakes. *J. Atmos. Sol. Terr. Phys.* **2003**, *65*, 391–407. [CrossRef]
5. Rapoport, Y.; Gotynyan, O.; Ivchenko, V.; Hayakawa, M.; Grimalsky, V.; Koshevaya, S.; Juarez-R, D. Modeling electrostatic-photochemistry seismoionospheric coupling in the presence of external currents. *Phys. Chem. Earth Parts A/B/C* **2006**, *31*, 437–446. [CrossRef]
6. Kuo, C.L.; Huba, J.D.; Joyce, G.; Lee, L.C. Ionosphere plasma bubbles and density variations induced by pre-earthquake rock currents and associated surface charges. *J. Geophys. Res. Space Phys.* **2011**, *116*. [CrossRef]
7. Meek, C.; Manson, A.; Martynenko, S.; Rozumenko, V.; Tyrnov, O. Remote sensing of mesospheric electric fields using MF radars. *J. Atmos. Sol. Terr. Phys.* **2004**, *66*, 881–890. [CrossRef]
8. Martynenko, S.I.; Clifford, S.F. On the electrical coupling between the troposphere and the mesosphere. *Int. J. Geomagn. Aeron.* **2006**, *6*, 2007. [CrossRef]
9. Haken, G. *Information and Self-Organization: A Macroscopic Approach to Complex Systems*; Komkniga: Moscow, Russia, 2005; 248p.
10. Mareev, E.A. Formation of Charge Layers in the Planetary Atmospheres. *Space Sci. Rev.* **2008**, *137*, 373–397. [CrossRef]
11. Denisenko, V.V.; Bychkov, V.V.; Pomozov, E.V. Calculation of atmospheric electric fields penetrating from the ionosphere. *Geomagn. Aeron.* **2009**, *49*, 1275–1277. [CrossRef]
12. Chum, J.; Liu, J.-Y.; Laštovička, J.; Fiser, J.; Mošna, Z.; Baše, J.; Sun, Y.-Y. Ionospheric signatures of the April 25, 2015 Nepal earthquake and the relative role of compression and advection for Doppler sounding of infrasound in the ionosphere. *Earth Planets Space* **2016**, *68*, 24. [CrossRef]
13. Yan, R.; Parrot, M.; Pinçon, J.-L. Statistical Study on Variations of the Ionospheric Ion Density Observed by DEMETER and Related to Seismic Activities. *J. Geophys. Res. Space Phys.* **2017**, *122*, 421–429. [CrossRef]
14. Denisenko, V.V.; Pomozov, E.V.; Denisenko, V.V.; Pomozov, E.V. Penetration of electric field from the near ground atmospheric layer to the ionosphere. *Geomagn. Aeron.* **2011**, *51*, 866–872. [CrossRef]
15. Rapoport, Y.; Grimalsky, V.; Krankowski, A.; Pulinets, S.; Fedorenko, A.; Petrishchevskii, S. Algorithm for modeling electromagnetic channel of seismo-ionospheric coupling (SIC) and the variations in the electron concentration. *Acta Geophys.* **2019**, *68*, 253–278. [CrossRef]
16. Rapoport, Y.; Grimalsky, V.; Fedun, V.; Agapitov, O.; Bonnell, J.; Grytsai, A.; Milinevsky, G.; Liashchuk, A.; Rozhnoi, A.; Solovieva, M.; et al. Model of propagation of VLF beams in the waveguide Earth-Ionosphere. Principles of tensor impedance method in multilayered gyrotropic waveguides. *Ann. Geophys.* **2020**, *38*, 207–230. [CrossRef]
17. Ampferer, M.; Denisenko, V.V.; Hausleitner, W.; Krauss, S.; Stangl, G.; Boudjada, M.Y.; Biernat, H.K. Decrease of the electric field penetration into the ionosphere due to low conductivity at the near ground atmospheric layer. *Ann. Geophys.* **2010**, *28*, 779–787. [CrossRef]
18. Kelley, M.C. *The Earth's Ionosphere Plasma Physics and Electrodynamics*; Academic Press: Amsterdam, The Netherlands, 2009; 556p.

19. Gonzales, C.A.; Kelley, C.; Fejer, B.G. Equatorial electric field during magnetically disturbed conditions. 2. Implifications of simultaneous auroral and equatorial measurements. *J. Geophys. Res.* **1979**, *84*, 5803–5813. [CrossRef]
20. Shah, M.; Jin, S. Statistical characteristics of seismo-ionospheric GPS TEC disturbances prior to global Mw $\geq$ 5.0 earthquakes (1998–2014). *J. Geodyn.* **2015**, *92*, 42–49. [CrossRef]
21. Thomas, J.N.; Huard, J.; Masci, F. A statistical study of global ionospheric map total electron content changes prior to occurrences of M $\geq$ 6.0 earthquakes during 2000–2014. *J. Geophys. Res. Space Phys.* **2017**, *122*, 2151–2161. [CrossRef]
22. Fuks, I.; Shubova, R.; Martynenko, S. Lower ionosphere response to conductivity variations of the near-earth atmosphere. *J. Atmos. Sol. Terr. Phys.* **1997**, *59*, 961–965. [CrossRef]
23. Pulinets, S.; Ouzounov, D. *The Possibility of Earthquake Forecasting*; IOP Publishing: Bristol, UK, 2018.
24. Parrot, M.; Tramutoli, V.; Liu, T.J.Y.; Pulinets, S.; Ouzounov, D.; Genzano, N.; Lisi, M.; Hattori, K.; Namgaladze, A. Atmospheric and ionospheric coupling phenomena associated with large earthquakes. *Eur. Phys. J. Spec. Top.* **2021**, *230*, 197–225. [CrossRef]
25. Sharma, S.; Singh, R.P.; Pundhir, D.; Singh, B. A multi-experiment approach to ascertain electromagnetic precursors of Nepal earthquakes. *J. Atmos. Sol. Terr. Phys.* **2020**, *197*, 105163. [CrossRef]
26. Zhang, X.; Wang, Y.; Boudjada, M.; Liu, J.; Magnes, W.; Zhou, Y.; Du, X. Multi-Experiment Observations of Ionospheric Disturbances as Precursory Effects of the Indonesian Ms6.9 Earthquake on 05 August 2018. *Remote Sens.* **2020**, *12*, 4050. [CrossRef]
27. Oyama, K.-I.; Kakinami, Y.; Liu, J.Y.; Abdu, M.A.; Cheng, C.Z. Latitudinal distribution of anomalous ion density as a precursor of a large earthquake. *J. Geophys. Res. Space Phys.* **2011**, *116*, 27. [CrossRef]
28. Pulinets, S.A.; Boyarchuk, K.A. *Ionospheric Precursors of Earthquakes*; Springer: Berlin/Heidelberg, Germany, 2004; 315p.
29. Hegai, V. Analytical model of a seismogenic electric field according to data of measurements in the surface layer of the midlatitude atmosphere and calculation of its magnitude at the ionospheric level. *Geomagn. Aeron.* **2020**, *60*, 507–520.
30. Rapoport, Y.; Grimalsky, V.; Hayakawa, M.; Ivchenko, V.; Juarez-R, D.; Koshevaya, S.; Gotynyan, O. Change of ionospheric plasma parameters under the influence of electric field which has lithospheric origin and due to radon emanation. *Phys. Chem. Earth Parts A/B/C* **2004**, *29*, 579–587. [CrossRef]
31. Rapoport, Y.; Gotynyan, O.; Ivchenko, V.; Kozak, L.; Parrot, M. Effect of acoustic-gravity wave of the lithospheric origin on the ionospheric F region before earthquakes. *Phys. Chem. Earth Parts A/B/C* **2004**, *29*, 607–616. [CrossRef]
32. Ouzounov, D.; Pulinets, S.; Hattori, K.; Taylor, P. *Pre-Earthquake Processes: A Multi-Disciplinary Approach to Earthquake Prediction Studies*; John Wiley & Sons: Hoboken, NJ, USA, 2018.
33. Rapoport, Y.; Hayakawa, M.; Gotynyan, O.; Ivchenko, V.; Fedorenko, A.; Selivanov, Y. Stable and unstable plasma perturbations in the ionospheric F region, caused by spatial packet of atmospheric gravity waves. *Phys. Chem. Earth Parts A/B/C* **2009**, *34*, 508–515. [CrossRef]
34. Pulinets, S. The synergy of earthquake precursors. *Earthq. Sci.* **2011**, *24*, 535–548. [CrossRef]
35. Vainshtein, L.A. *Open Resonators and Open Waveguides*; Golem Press: Boulder, CO, USA, 1969; 439p.
36. Vershinin, E.F.; Buzevich, A.V.; Yumoto, K.; Saita, K.; Tanaka, Y. Correlations of Seismic Activity with Electromagnetic Emissions and Variations in Kamchatka Region. In *Atmospheric and Ionospheric Electromagnetic Phenomena Associated with Earthquakes*; Hayakawa, M., Ed.; Terrapub: Tokyo, Japan, 1999; pp. 513–517.
37. Choudhury, A.; Guha, A.; De, B.K.; Roy, R. A statistical study on precursory effects of earthquakes observed through the atmospheric vertical electric field in northeast India. *Ann. Geophys.* **2013**, *56*, R0331. [CrossRef]
38. Martynenko, S.; Rozumenko, V.; Tsymbal, A.; Tyrnov, O.; Gokov, A. Mesospheric electric field measurements with a partial reflection radar. *J. Atmos. Electr.* **1999**, *19*, 81–86. [CrossRef]
39. Gurevich, A.V. *Nonlinear Phenomena in the Ionosphere*; Springer: New York, NY, USA, 1978.
40. Liu, J.-Y.; Chao, C.-K. An observing system simulation experiment for FORMOSAT-5/AIP detecting seismo-ionospheric precursors. *Terr. Atmos. Ocean. Sci.* **2017**, *28*, 117–127. [CrossRef]
41. Namgaladze, A.A.; Zolotov, O.V.; Zakharenkova, I.E.; Shagimuratov, I.I.; Martynenko, O.V. Ionospheric total electron content variations observed before earthquakes: Possible physical mechanism and modeling. *Proc. MSTU* **2009**, *12*, 308–315.
42. Trakhtengertz, V.Y.; Mareev, E.A.; Sorokin, A.E. Electrodynamics of a convective cloud. *Radiophys. Quantum Electron.* **1997**, *40*, 77–86. [CrossRef]
43. Kotsarenko, N.Y.; Rapoport, Y.G.; Redkoborodyj, Y.N.; Shvidkij, A.A. Instability of acoustic-gravity waves in an atmosphere with impurities which release and absorb heat. *Kinemat. Phys. Celest. Bodies* **1994**, *10*, 61–64.
44. Domnin, I.; Emelyanov, L.; Kotov, D.; Panasenko, S.; Chernogor, L.; Lyashenko, M.; Bogomaz, O. Results of experimental and theoretical studies of physical processes in the ionosphere over Ukraine in 2018–2020. In *Space Research in Ukraine. 2019–2020*; Fedorov, O., Ed.; Akademperiodyka: Kyiv, Ukraine, 2020; pp. 43–50.
45. Denisenko, V.; Ampferer, M.; Pomozov, E.; Kitaev, A.; Hausleitner, W.; Stangl, G.; Biernat, H. On electric field penetration from ground into the ionosphere. *J. Atmos. Sol. Terr. Phys.* **2013**, *102*, 341–353. [CrossRef]
46. Denisenko, V.V.; Nesterov, S.A.; Boudjada, M.Y.; Lammer, H. A mathematical model of quasistationary electric field penetration from ground to the ionosphere with inclined magnetic field. *J. Atmos. Sol. Terr. Phys.* **2018**, *179*, 527–537. [CrossRef]
47. Denisenko, V.V.; Boudjada, M.Y.; Horn, M.; Pomozov, E.V.; Biernat, H.K.; Schwingenschuh, K.; Lammer, H.; Prattes, G.; Cristea, E. Ionospheric conductivity effects on electrostatic field penetration into the ionosphere. *Nat. Hazards Earth Syst. Sci.* **2008**, *8*, 1009–1017. [CrossRef]
48. Samarskii, A.; Radulescu, V. Theory of Difference Schemes. *Appl. Mech. Rev.* **2002**, *55*, B24–B25. [CrossRef]

49. Samarskii, A.A.; Nikolaev, E.S. *Numerical Methods for Grid Equations*; Birkhäuser Verlag: Basel, Switzerladnd, 1989; Volume 2.
50. Marchuk, G.I. Splitting and Alternating Direction Methods. In *Handbook of Numerical Analysis*; Ciarlet, P.G., Lions, J.L., Eds.; Elsevier: Amsterdam, The Netherlands, 1990; Volume 1, pp. 197–462.
51. Alperovich, L.S.; Fedorov, E.N.; Alperovich, P.L.S.; Fedorov, P.E.N. *Hydromagnetic Waves in the Magnetosphere and the Ionosphere*; Springer: Dordrecht, The Netherlands, 2007; 426p.
52. Guglielmi, A.V.; Pokhotelov, O.A. *Geoelectromagnetic Waves*; CRC Press: Boca Raton, FL, USA, 1996; 382p.
53. Sorokin, V.; Chmyrev, V.; Isaev, N. A generation model of small-scale geomagnetic field-aligned plasma inhomogeneities in the ionosphere. *J. Atmos. Sol. Terr. Phys.* **1998**, *60*, 1331–1342. [CrossRef]
54. Chernogor, L.F. *Physics and Ecology of Catastrophes*; V.N. Karazin Kharkiv National University: Kharkiv, Ukraine, 2012; 556p. (In Russian)
55. Sorokin, V.; Isaev, N.; Yaschenko, A.; Chmyrev, V.; Hayakawa, M. Strong DC electric field formation in the low latitude ionosphere over typhoons. *J. Atmos. Sol. Terr. Phys.* **2005**, *67*, 1269–1279. [CrossRef]
56. Chernogor, L.F.; Rozumenko, V.T. Earth–Atmosphere–Geospace as an Open Nonlinear Dynamical System. *Radio Phys. Radio Astron.* **2008**, *13*, 120–137.
57. Chernogor, L.F. The Earth–Atmosphere–Geospace System: Main Properties and Processes. *Int. J. Remote Sens.* **2011**, *32*, 3199–3218. [CrossRef]
58. Vanina-Dart, L.B.; Sharkov, E.A. Main results of recent investigations into the physical mechanisms of the interaction of tropical cyclones and the ionosphere. *Izv. Atmos. Ocean. Phys.* **2016**, *52*, 1120–1127. [CrossRef]
59. Simpson, J.; Halverson, J.B.; Ferrier, B.S.; Petersen, W.A.; Simpson, R.H.; Blakeslee, R.; Durden, S.L. On the Role of "Hot Towers" in Tropical Cyclone Formation. *Meteorol. Atmos. Phys.* **1998**, *67*, 15–35. [CrossRef]
60. Qie, X.; Liu, D.; Sun, Z. Recent advances in research of lightning meteorology. *J. Meteorol. Res.* **2014**, *28*, 983–1002. [CrossRef]
61. Bondur, V.G.; Pulinets, S.A. Effect of mesoscale atmospheric vortex processes on the upper atmosphere and ionosphere of the Earth. *Izv. Atmos. Ocean. Phys.* **2012**, *48*, 871–878. [CrossRef]
62. Nina, A.; Radovanović, M.; Milovanović, B.; Kovačević, A.; Bajčetić, J.; Popović, L.Č. Low ionospheric reactions on tropical depressions prior hurricanes. *Adv. Space Res.* **2017**, *60*, 1866–1877. [CrossRef]
63. Al'pert, Y.L. *Propagation of Electromagnetic Waves and the Ionosphere*; Nauka: Moscow, Russia, 1972; 563p. (In Russian)
64. Schunk, R.W.; Nagy, A.F. *Ionospheres, Physics, Plasma Physics, and Chemistry*; Cambridge University Press: Cambridge, UK, 2010; 628p.
65. Jursa, A.S. (Ed.) *Handbook of Geophysics and the Space Environment*; Air Force Geophysics Laboratory: Hanscom AFB, MA, USA, 1985; 1042p.
66. Sugakov, V.I. *Electrodynamics*; Vyshcha Shkola: Kyiv, Ukraine, 1974; 272p. (In Ukrainian)
67. Sorokin, V.M.; Yaschenko, A.K.; Hayakawa, M. A perturbation of DC electric field caused by light ion adhesion to aerosols during the growth in seismic-related atmospheric radioactivity. *Nat. Hazards Earth Syst. Sci.* **2007**, *7*, 155–163. [CrossRef]
68. Dobrovolsky, I.P.; Zubkov, S.I.; Miachkin, V.I. Estimation of the size of earthquake preparation zones. *Pure Appl. Geophys.* **1979**, *117*, 1025–1044. [CrossRef]
69. Wang, C.; Zhang, J.J.; Tang, B.; Fu, S.Y. Comparison of equivalent current systems for the substorm event of 8 March 2008 derived from the global PPMLR-MHD model and the KRM algorithm. *J. Geophys. Res. Space Phys.* **2011**, *116*, 07207. [CrossRef]
70. Rabinovich, M.I.; Trubetskov, D.I. *Oscillations and Waves in Linear and Nonlinear Systems*; Kluwer Academic Publishers: Dordrecht, The Netherlands; Boston, MA, USA; London, UK, 1989; 577p.
71. Vainshtein, L.A. *Electromagnetic Waves*; Nauka: Moscow, Russia, 1988; 440p. (In Russian)
72. Felsen, L.B.; Marcuvitz, N. *Radiation and Scattering of Waves*; Mir: Moscow, Russia, 1978. (In Russian)
73. Isaev, N.V.; Sorokin, V.M.; Chmyrev, V.M.; Serebryakova, O.N. Ionospheric electric fields related to sea storms and typhoons. *Geomagn. Aeron.* **2002**, *48*, 638–643.
74. Freund, F. Toward a unified solid state theory for pre-earthquake signals. *Acta Geophys.* **2010**, *58*, 719–766. [CrossRef]
75. Scoville, J.; Sornette, J.; Freund, F.T. Paradox of peroxy defects and positive holes in rocks Part II: Outflow of electric currents from stressed rocks. *J. Asian Earth Sci.* **2015**, *114*, 338–351. [CrossRef]